1963-09-03

Analysis of the Transit Response of a Flat Rotating Disk by Generalized Transforms

Kenneth Wayne Chase
Brigham Young University - Provo

ANALYSIS OF THE TRANSIENT RESPONSE OF A FLAT

ROTATING DISK BY GENERALIZED TRANSFORMS

A Thesis

Presented to the

Department of Mechanical Engineering

Brigham Young University

In Partial Fulfillment

of the Requirements for the Degree

Master of Science

by

Kenneth Wayne Chase

September 3, 1963

This thesis by Kenneth Wayne Chase, is accepted in its present form by the Department of Mechanical Engineering of Brigham Young University as satisfying the thesis requirements for the degree of Master of Science.

September 3, 1963
Date

Typed by Gloria Chase

ACKNOWLEDGEMENTS

TABLE OF CONTENTS

LIST OF TABLES

LIST OF ILLUSTRATIONS

NOMENCLATURE

r, θ	Polar coordinates
h	Thickness
σ_r, σ_θ	Normal stress
$\tau_{r\theta}$	Shear stress
R, T	Radial and tangential body forces per unit volume
$\epsilon_r, \epsilon_\theta$	Normal strain
$\gamma_{r\theta}$	Shear strain
u, v	Displacements in the radial and tangential directions
ν	Poisson's ratio
E	Modulus of elasticity
G	Shear modulus
a	Inside radius of disk
b	Outside radius of disk
Ω	Angular velocity
ω	Angular velocity; natural frequency of vibration
$\propto$	Angular acceleration
x	Non-dimensional radial coordinate
τ	Non-dimensional time
$\bar{u}, \bar{v}$	Non-dimensional displacements
F_s, c_s	Dimensionless dynamic similarity parameters
T_x	Finite Hankle transform operator
L_t	Laplace transform operator
K, N	Kernel functions for integral transforms

$C(\lambda), D(\beta)$	Normalizing factors
λ_n, β_m	Extensional and torsional eigenvalues
J_1, Y_1	Bessel functions of 1st and 2nd kinds of order one
H_1, H_2	Finite Hankle transform of x
$\eta(t), \xi(t)$	Superposition integrals from the transient response
$c_1, c_2,$	Stress wave propagation velocities
m_n	Exponent of empirical frequency equation
B_n	Coefficient of empirical frequency equation
r_{xy}	Correlation coefficient

Subscripts

r, x, t	Partial differentiation
o	Initial conditions

Superscripts

x, t	Integral transformation

I. INTRODUCTION

The object of this thesis was to lay a foundation for
a comprehensive study of the dynamic response of rotating
members. This initial phase of the study includes a theoret-
ical investigation and proposes experimental techniques for
the determination of the stresses and strains in a thin,
rotating disk with a concentric hole, subjected to transient
shaft inputs. There are many practical applications of this
problem including computor memory storage disks, turbine
rotors, grinding wheels, saw blades, gears, optical reflect-
ors, and solar sails for space vehicles.

The solution for any forced vibration or transient
response problem in the vibration of continuous media can be
expressed as a series expansion in terms of the mode shapes
and natural frequencies for free vibration. Previous theo-
retical investigations have been concerned with solving the
free vibration problem to determine the natural frequencies
and mode shapes for application to steady-state forced vi-
brations. Very little numerical data has been obtained for
the case of in-plane vibrations and basic discrepancies exist
between the findings of individual investigators. This
thesis applies the method of generalized integral transforms
to the in-plane vibration problem and obtains an exact
solution for the transient response of a rotating disk to

time-varying shaft inputs. The response has been expressed in terms of superposition integrals containing the general shaft inputs. The integrals have been evaluated for three specific inputs, chosen to approximate the expected results of the proposed experimental phase.

To aid in obtaining a numerical solution, numerical data for the natural frequencies, nodes, and mode shapes of vibration have been obtained and empirical formulas for the frequencies have been derived. This data is more complete than previously published results and serves to settle the differences that have occurred.

In addition, an attempt has been made to organize some of the literature and list some of the problems related to an experimental investigation, as well as to make recomendations on techniques.

MATHEMATICAL MODEL

A disk of uniform thickness with a concentric hole was considered clamped to an infinitely rigid shaft and subjected to a general time-varying shaft input. The loading was assumed to be pure shear and axially symmetric. The disk consisted of homogeneous, isotropic, linearly elastic material and all surfaces were free from stress or any means of support except for the inner radius.

The radius of the disk was assumed large compared with the thickness, so that thickness modes of vibration might be neglected. All stresses were assumed uniformly

distributed across the thickness of the disk. In other words, the two-dimensional theory of elasticity was applicable. Creep, stress concentrations, residual stresses, etc, were not considered. Furthermore, in the vibration analysis, the oscillations were limited to small elastic deformations from the steady-state deformation due to the initial angular velocity.

SURVEY OF STUDIES ON DISKS

Stresses and Free Vibration of Non-Rotating Disks.
One of the earliest considerations of the vibrations of a circular disk was the study by Kirchhoff, in 1850, of the free transverse vibrations of a solid disk for two cases-- free outer edge and clamped outer edge. He found that there were two independent sets of nodes (non-vibrating points), one forming a pattern of concentric circles, the other made up of diameters forming a symmetrical "wagon-wheel" pattern. His results are reproduced and discussed on pages 359-371 in Lord Rayliegh's Theory of Sound. [10][1] Included are experimental and theoretical values of the nodal circle radii for the case of no nodal diameters.

The in-plane free vibrations of a solid disk were considered by Love [5] in his well-known treatise on elasticity. He found the transcendental frequency equations in terms of Bessel functions for the torsional and radially

---

[1] Numbers in brackets refer to references in the bibliography .

extensional modes from two-dimensional theory of elasticity,
but calculated no numerical results. Recently, Nowak [8]
calculated these natural frequencies for the extensional
modes (without nodal diameters), using both the series expan-
sion for Bessel functions and the large value approximations
in terms of trigonometric functions. The two sets of fre-
quencies agreed rather well, except for the lower frequen-
cies. He also gave a physical interpretation for the singu-
larity that appears at the origin.

The fundamental (lowest natural) frequency of flex-
ural vibrations for a disk with a concentric hole (annulus)
was determined analytically from two-dimensional theory of
elasticity by Raju [9] for nine different combinations of
boundary conditions and for zero, one, or two nodal diam-
eters, with the discovery that the lowest number of nodal
diameters did not always produce the lowest frequency.

Since 1950, a great deal of effort has been concen-
trated on determining the effect of thickness on the natural
frequency spectrum. This interest has primarily been in-
spired by the use of transversely vibrating disks in tele-
phones and in mechanical filters. Experiments by E.A.G.
Shaw [12] stimulated considerable activity in this area,
which has continued to the present time. Shaw used the
piezoeletric effect to excite the flexural and thickness
vibration modes of thick barium titanate disks which had
been silver surfaced. He found that only the axially sym-
metric modes could be excited strongly and reported a definite
coupling between the flexural and thickness vibrations at

natural frequencies near those of thickness vibration.

There are at least two distinct thickness modes of vibration: the "thickness shear" mode, produced by relative angular motion between planes parallel to the face of the disk and the "thickness compression" mode, an alternate expansion and contraction in thickness due to the Poisson effect. The frequency equation for these two modes of vibration was determined analytically by Aggarwal [1], who found a definite influence when excited with the extensional and flexural vibrations.

Mindlin, with several co-workers, published a series of papers on the analytical determination of thickness effects. They discussed coupling effects between:
1. flexural and thickness shear modes [2,6]
2. extensional and thickness-compression modes
3. extensional modes and thickness-compression and thickness-shear modes [3]

The effect of Poisson's ratio on the natural frequency of flexural vibrations was demonstrated analytically and experimintally by Sharma [11] using the thickness-shear corrected theory.

Most of the foregoing papers attempted to improve the theory of vibrations in disks and circular plates by using three-dimensional theory of elasticity. An alternate approach is to start with plane stress theory and add correction terms. This method was used by Mosely [7] to correct the radially extensional natural frequencies for

thickness-compression effects. The correction factor was derived by taking the ratio of the kinetic energy of the disk with axial motion due to the Poisson effect, to the kinetic energy neglecting this effect.

Stress and Free Vibrations in Rotating Disks. The advent of turbo-machinery stimulated interest in the effects of rotational velocities on the stresses and vibrations of disks. The natural frequencies were needed, so that dangerous resonant vibrations of rotors could be eliminated. Among the first to attempt an analytical investigation were Lamb and Southwell [19,24] who, in 1921, considered the change in frequency of transverse vibrations, neglecting flexural forces, for a solid disk and an annulus clamped to a rigid hub.

A comprehensive study of steady-state stresses and free vibrations of rotating disks was published by Biezeno and Grammel in 1939. [13] They derived two-dimensional differential equations of motion in terms of stresses and displacements for disks of varying thickness, with uniform disks as a special case. Frequency equations for extensional, torsional, and flexual vibrations were determined for a number of particular cases, both with and without diametral nodes. A detailed discussion was included of the manner by which the number and spacing of rotor and stator blades may result in forced vibration of the rotor disk. Mathematical models were contrived to simulate the affect of shrink-fitted drive shafts and blades mounted on the periphery of

the disk. Also, a discussion was presented on the natural frequency of vibration of rotor blades and their subsequent effect on vibrations of disks. Among their conclusions were the following:

1. Coriolis acceleration has a negligible effect on the natural frequencies of vibration.

2. Vibrations with no diametral nodes are most critical, because the frequencies are generally lower and the amplitudes higher.

3. Vibrations with no circular nodes are most critical for the same reasons.

An experimental determination of centrifugal stresses was made by Frost and Whitcomb [14] utilizing the "stress freezing" technique of photoelasticity, in which a photoelastic model was heated to a plastic state while rotating at a constant velocity, then cooled slowly with the model still rotating, causing it to "set" in its deformed state. The model was then analyzed by conventional photoelastic methods. This technique has since been extended to disks with simulated rotor blades, hubs, discontinuities, etc. [15,16,18,20]

Two interesting analyses of the steady-state stresses and deformations were conducted by Owen [21], who determined the solution for a disk rotated at a constant velocity such that the centrifugal stresses were in the plastic range of the disk material, and by Karas [17], who determined the solution for disks of various thickness profiles subjected

to a constant angular acceleration.

Another two-dimensional analysis of the in-plane free vibrations was made by Singh and Nandeeswaraiya [23]. They began with Biezeno and Grammel's differential equations, accepting their assumption of negligible coupling due to coriolis, and solved them for two cases--a disk with a rigid hub and a disk with a free inner edge--to bracket the effect of press fits and the inertial effect of blading. Numerical values were calculated to two digits for outside-to-inside diameter ration from 1.6 to ∞.

More recently, a solution for the in-plane vibrations was determined by Simmonds. [22] He derived his own differential equations and concluded that the coupling terms were negligible. Solutions were obtained for the frequency equations and natural frequencies for the same two limiting cases as Singh and Nandeeswaraiya. Numerical values for the first three natural frequencies have been tabulated to four decimal places for each case, for inside-to-outside diameter ratios from 0 to 1 and for zero and one diametral node. Three values of Poisson's ratio were included to demonstrate its effects on frequency. Simmond's torsional frequencies agree with those of Singh and Nandeeswaraiya [23], but there was considerable disagreement in the extensional frequencies.

II. DERIVATION OF GOVERNING EQUATIONS

EQUATIONS OF MOTION

Dynamic Equilibrium. Beginning with a general differential element in polar coordinates as in Fig. 1, the equations of motion were derived following the method of Timoshenko and Goodier. [25] D'Alembert's principle was applied to reduce the dynamic equations to those of static equilibrim. Equating forces in the radial and tangential directions and neglecting terms of second order, the equations of motion in terms of stress were found to be:

$$\frac{\partial \sigma_r}{\partial r} + \frac{1}{r}\left(\sigma_r - \sigma_\theta\right) + \frac{1}{r}\frac{\partial \tau_{r\theta}}{\partial \theta} + R = 0 \tag{1}$$

$$\frac{\partial \tau_{r\theta}}{\partial r} + \frac{2}{r}\tau_{r\theta} + \frac{1}{r}\frac{\partial \sigma_\theta}{\partial \theta} + T = 0 \tag{2}$$

where σ_r and σ_θ are the radial and tangential normal stresses, $\tau_{r\theta}$ is the shear stress, and R and T are, respectively, the radial and tangential body forces per unit volume.

From Hooke's Law for plane stress, the stresses may be expressed in terms of the strains ϵ_r, ϵ_θ and $\gamma_{r\theta}$ which represent strains in the radial, tangential, and shear directions respectively. These relations are as follows:

$$\left.\begin{aligned}
\sigma_r &= \frac{E}{1-\nu^2}\left(\epsilon_r + \nu\epsilon_\theta\right)\\[2mm]
\sigma_\theta &= \frac{E}{1-\nu^2}\left(\epsilon_\theta + \nu\epsilon_r\right)\\[2mm]
\tau_{r\theta} &= G\,\gamma_{r\theta}
\end{aligned}\right\} \tag{3}$$

where ν is Poisson's ratio, E is Young's Modulus and G is the shear modulus.
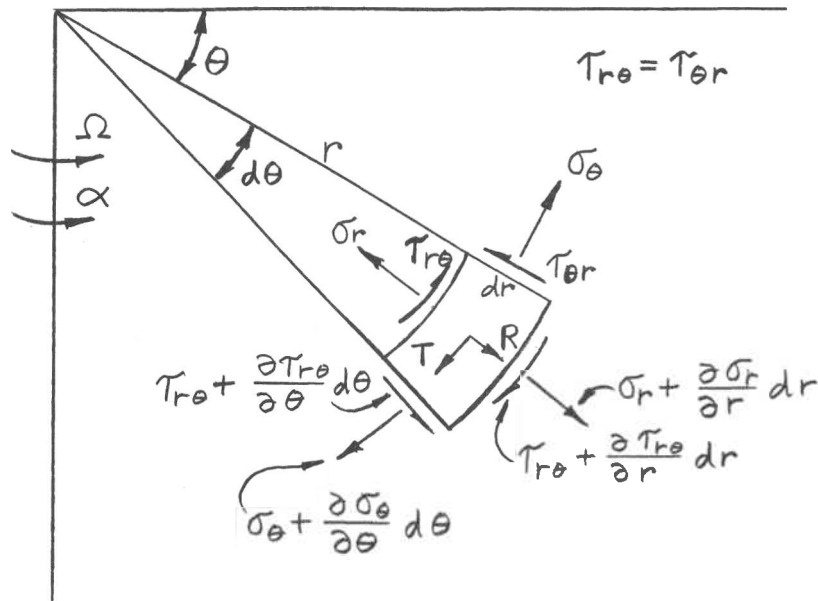
Figure 1. Differential element of an elastic body in polar corrdinates.

Proceeding with the development in reference 25, denoting the displacement in the radial direction by u and the tangential direction by v, the strains may be expressed in terms of the displacements as follows:

$$\epsilon_r = \frac{\partial u}{\partial r}$$

$$\epsilon_\theta = \frac{u}{r} + \frac{1}{r}\frac{\partial v}{\partial \theta}$$

$$\gamma_{r\theta} = \frac{1}{r}\frac{\partial u}{\partial \theta} + \frac{\partial v}{\partial r} - \frac{v}{r}$$

(4)

Bodies with Axial Symmetry. For bodies with axial symmetry, the partial deratives with respect to θ are zero and equations (1), (2), and (4) become:

$$\frac{\partial \sigma_r}{\partial r} + \frac{1}{r}(\sigma_r - \sigma_\theta) + R = 0$$

$$\frac{\partial T_{r\theta}}{\partial r} + \frac{2}{r} T_{r\theta} + T = 0$$

$$\qquad (5)$$

$$\epsilon_r = \frac{\partial u}{\partial r}$$

$$\epsilon_\theta = \frac{u}{r}$$

$$\gamma_{r\theta} = \frac{\partial v}{\partial r} - \frac{v}{r}$$

$$\qquad (6)$$

Substituting equations (6) into equations (3) we obtain an expression for the stresses in terms of displacements.

$$\sigma_r = \frac{E}{1-\nu^2}\left[\frac{\partial u}{\partial r} + \nu \frac{u}{r}\right]$$

$$\sigma_\theta = \frac{E}{1-\nu^2}\left[\frac{u}{r} + \nu \frac{\partial u}{\partial r}\right]$$

$$T_{r\theta} = G\left[\frac{\partial v}{\partial r} - \frac{v}{r}\right]$$

$$\qquad (7)$$

And substituting equations (7) into the equations of motion (5), we obtain the equations of motion in terms of displacements and general body forces:

$$\frac{\partial^2 u}{\partial r^2} + \frac{1}{r}\frac{\partial u}{\partial r} - \frac{u}{r^2} + \frac{1-\nu^2}{E} R = 0 \qquad (8)$$

$$\frac{\partial^2 v}{\partial r^2} + \frac{1}{r}\frac{\partial v}{\partial r} - \frac{v}{r^2} + \frac{1}{G} T = 0 \qquad (9)$$

Compatibility. In any problem in elasticity, a third equation in terms of displacements often arises from the relation between the strains. This relation must be satisfied so that the solution for the strains will be compatible.

On examining the expression for strain (6) it was discovered that no relation exists between the normal strains, ϵ_r and ϵ_θ and the shear strain, $\gamma_{r\theta}$, because the former are in terms of u only and the latter is in terms of v only. However, there was a relation between ϵ_r and ϵ_θ which must be satisfied. Taking the partial derivative of ϵ_θ we obtain:

$$\frac{\partial \epsilon_\theta}{\partial r} = \frac{\partial}{\partial r}\left(\frac{u}{r}\right) = \frac{1}{r}\frac{\partial u}{\partial r} - \frac{u}{r^2}$$
$$= \frac{1}{r}\left(\frac{\partial u}{\partial r} - \frac{u}{r}\right)$$

Substituting for each term, its corresponding strain from equations (6) produces a relation between the normal strains:

$$\frac{\partial \epsilon_\theta}{\partial r} = \frac{1}{r}\left(\epsilon_r - \epsilon_\theta\right) \tag{10}$$

By Hooke's Law, the strains in terms of the stresses are:

$$\epsilon_r = \frac{1}{E}\left(\sigma_r - \nu\,\sigma_\theta\right)$$

$$\epsilon_\theta = \frac{1}{E}\left(\sigma_\theta - \nu\,\sigma_r\right)$$

Substituting these relations into (10) we get:

$$\frac{\partial \sigma_\theta}{\partial r} - \nu \frac{\partial \sigma_r}{\partial r} = \frac{1}{r}\left[\sigma_r - \sigma_\theta + \nu(\sigma_r - \sigma_\theta)\right]$$

which may be written as:

$$\frac{\partial \sigma_\theta}{\partial r} - \frac{1}{r}(\sigma_r - \sigma_\theta) = \nu\left[\frac{\partial \sigma_r}{\partial r} + \frac{1}{r}(\sigma_r - \sigma_\theta)\right] \qquad (11)$$

Substituting the first equation of equations (5) into the right hand side of (11):

$$\frac{\partial \sigma_\theta}{\partial r} - \frac{1}{r}(\sigma_r - \sigma_\theta) = -\nu R \qquad (12)$$

Now by substituting equations (7), this equation may be expressed in terms of displacements:

$$\frac{\partial^2 u}{\partial r^2} + \frac{1}{r}\frac{\partial u}{\partial r} - \frac{u}{r^2} + \frac{1-\nu^2}{E} R = 0$$

which is identical to equation(8), therefore, no additional relation exists due to compatibility.

BODY FORCES AND BOUNDARY CONDITIONS

Body Forces. The body forces per unit volume, R and T, acting on the differential element of Fig. 1. are, by Newton's Second Law, equal to the density of the element multiplied by the acceleration, and by D'Alembert's principle they are opposite in sense.

$$\frac{F}{vol} = \rho(a_r i + a_t j)$$

where: a_r = radial acceleration

a_t = tangential acceleration

$\bar{i}$ and $\bar{j}$ = unit vectors.

ρ = density of the material

Determination of Acceleration. The acceleration vector, $\bar{A}_P$ of an arbitrary point P, located at radius r_P on the disk, may be obtained by a consideration of the theory of rigid body dynamics for a particle referred to a rotating reference system. Consider an xyz reference coordinate at-tatched to a rotating disk, with its origin at the center of the disk. The disk is deformed due to the initial angular velocity ω_o. Then, as the angular velocity is changed to $\Omega(t) = \omega_o + \omega(t)$ a displacement of the point P occurs in the radial and tangential directions, denoted by u and v, respectively. Letting i,j and k represent the unit vectors in the x,y, and z directions, the angular velocity vector is $\Omega\bar{k}$. Differentiating this with respect to time ($\dot{r}_P = 0$) gives the vector velocity :

$$\bar{V}_P = \dot{u}\,\bar{i} + (r_P + u)\dot{\bar{i}} + \dot{v}\bar{j} + v\dot{\bar{j}}$$

Where the dot indicated differentiation with respect to time and the bar indicates a vector quantity.

By vector analysis, the derivative of a vector, $\bar{S}$, is the cross product of the angular velocity vector and the vector $\bar{S}$, [41], so we may write $\dot{\bar{i}}$ and $\dot{\bar{j}}$ as:

$$\dot{\bar{i}} = \Omega\bar{k} \times \bar{i} = \Omega\bar{j}$$

and $\quad \dot{\bar{j}} = \Omega\bar{k} \times \bar{j} = -\Omega\bar{i}$

therefore, $\bar{V}_P$ can be written:

$$\bar{V}_P = (\dot{u} - \Omega v)\bar{i} + (\dot{v} + \Omega r_P + \Omega u)\bar{j}$$

Again taking the time derivative:

$$\bar{A}_P = \frac{d\bar{V}}{dt} = (\ddot{u} - \dot{\Omega}v - \Omega\dot{v})\bar{i} + (\dot{u} - \Omega v)\dot{\bar{i}}$$
$$+ (\ddot{V} + \dot{\Omega}r_p + \dot{\Omega}u + \dot{u})\bar{j} + (\dot{v} + \Omega r_p + \Omega u)\dot{\bar{j}}$$

Substituting for $\dot{\bar{i}}$ and $\dot{\bar{j}}$ and letting $\dot{\Omega} = \alpha$:

$$\bar{A}_P = (\ddot{u} - v\alpha - 2\Omega\dot{v} - r_p\Omega^2 - u\Omega^2)\bar{i}$$
$$+ (\ddot{V} + r_p\alpha + u\alpha + 2\Omega\dot{u} - v\Omega^2)\bar{j} \tag{13}$$

The body forces for any point on the disk are:

$$R = -\rho\, a_r$$
$$T = -\rho\, a_t$$

Substituting the acceleration components from (13):

$$R = -\rho(\ddot{u} - v\alpha - 2\Omega\dot{v} - r\Omega^2 - u\Omega^2)$$
$$T = -\rho(\ddot{V} + r\alpha + u\alpha + 2\Omega\dot{u} - v\Omega^2) \tag{14}$$

Boundary Conditions. As stated in Chapter I., the outer edge of the disk is completely unrestrained, therefore, the shear stress and stress normal to the edge are zero. From these conditions we obtain:

$$\sigma_r = \frac{E}{1-\nu^2}\left[u_r(b) + \frac{\nu}{b}u(b)\right] = 0$$
$$\tau_{r\theta} = G\cdot\left[v_r(b) - \frac{1}{b}v(b)\right] = 0 \tag{15}$$

where r equals b, the outside radius and the sub-script r denotes the partial derivative with respect to r.

At the inner edge of the disk, the displacements must be zero, since the disk is clamped to a rigid hub. The boundary conditions at r equals a, the inside radius are:

$$u(a) = 0$$
$$v(a) = 0 \tag{16}$$

Non-dimensionalized system of equations. A non-dimensional system of equations and boundary conditions was derived by introducing non-dimensional variables $x, \bar{u}$, and $\bar{v}$, defined as:

$$X = \frac{r}{a}, \quad \bar{u} = \frac{u}{a}, \quad \bar{V} = \frac{V}{a}$$

then, $\frac{\partial X}{\partial r} = \frac{1}{a}$

(17)

From the definition of a partial derivative, the derivatives of $u = f(x,t)$ are found in the following manner:

$$\frac{\partial u}{\partial r} = \frac{\partial u}{\partial X}\frac{\partial X}{\partial r} + \frac{\partial u}{\partial t}\frac{\partial t}{\partial r}^{0}$$

Substituting (18):

$$\frac{\partial u}{\partial r} = \frac{1}{a}\frac{\partial u}{\partial X}$$

(18)

Differentiating by the chain rule to find the second derivative and substituting (18):

$$\frac{\partial^2 u}{\partial r^2} = \frac{1}{a^2}\frac{\partial^2 u}{\partial X^2}$$

Similarly, it can be shown:

$$\frac{\partial V}{\partial r} = \frac{1}{a}\frac{\partial V}{\partial X}$$

$$\frac{\partial^2 V}{\partial r^2} = \frac{1}{a^2}\frac{\partial^2 V}{\partial X^2}$$

Also noting that $u = a\bar{u}$, $\frac{\partial u}{\partial X} = a\frac{\partial \bar{u}}{\partial X}$, $\frac{\partial^2 u}{\partial X^2} = a^2\frac{\partial^2 \bar{u}}{\partial X^2}$, etc., the differential equations (8) and (9) become:

$$\bar{u}_{XX} + \frac{1}{X}\bar{u}_X - \frac{1}{X^2}\bar{u} = -\frac{a^2}{E}(1-\nu^2)R$$

$$\bar{V}_{XX} + \frac{1}{X}\bar{V}_X - \frac{1}{X^2}\bar{V} = -\frac{a^2}{G}T$$

Finally, substituting the expressions (14) for the body forces, the system of equations and the boundary conditions may be written:

$$\bar{u}_{xx} + \frac{1}{x}\bar{u}_x - \frac{1}{x^2}\bar{u} = \rho\frac{a^2}{E}(1-\nu^2)\left[\bar{u}_{tt} - \alpha\bar{v}\right.$$
$$\left. -2\Omega\bar{v}_t - \Omega^2 x - \Omega^2\bar{u}\right]$$

$$\bar{u}(1,t) = 0$$

$$\bar{u}_x\left(\frac{b}{a}\right) + \frac{a}{b}\cdot\nu\,\bar{u}\left(\frac{b}{a}\right) = 0$$

$$\bar{u}(x,0) = \bar{u}_o$$

$$u_t(x,0) = 0$$

$$(19)$$

$$\bar{v}_{xx} + \frac{1}{x}\bar{v}_x - \frac{1}{x^2}\bar{v} =$$
$$\rho\frac{a^2}{G}\left[\bar{v}_{tt} + \alpha x + \alpha\bar{u} + 2\Omega\bar{u}_t - \Omega^2\bar{v}\right]$$

$$\bar{v}(1,t) = 0$$

$$\bar{v}_x\left(\frac{b}{a}\right) - \frac{a}{b}\bar{v}\left(\frac{b}{a}\right) = 0$$

$$\bar{v}(x,0) = 0$$

$$\bar{v}_t(x,0) = 0$$

$$(20)$$

III. SOLUTION BY GENERALIZED TRANSFORMS

GENERALIZED TRANSFORMS

<u>Definition</u>. The generalized or integral transform
with respect to x of a function of x is defined as:

$$T_x \left[f(x) \right] = \int_0^\infty f(x) \, K_n(\lambda_n, x) \, dx = F^x(\lambda_n) \tag{21}$$

where the range of values of x is from 0 to ∞. $Kn(\lambda_n, x)$
is known as the "kernel function" and is determined along
with the parameter λ_n by the form of the differential
equation and the boundary conditions. The application of
an integral transform to partial differential equations
results in a reduction in the number of independent vari-
ables, as can be seen in (21), since the transformed f(x) is
no longer a function of x, but a known function of λ_n.
In many physical problems, repeated transformations, using
a different kernel for each independent variable, can reduce
a differential equation in several variables to an algebraic
equation in terms of the boundary values and transformed
variables. The best known example of an integral transform
is the Laplace transform, often used to eliminate the time
variable in differential equations. It is defined as:

$$L_t \left[f(x,t) \right] = \int_0^\infty f(x,t) \, e^{-st} \, dt = F^t(x, s)$$

The greatest single factor limiting the use of integ-
ral transforms is the difficulty in obtaining an inverse

transform. The most common transforms have an inversion formula of the form:

$$f(x) = \int_0^\infty F^x(\lambda_n) \, H(\lambda_n, x) \, d\lambda_n$$

where H (λ, x) is the inversion kernel. It is desirable to find a symmetrical transform such that $K(\lambda, x) = H(\lambda, x)$. In most cases, this integral covers the complex plane of real and imaginary numbers and cannot be integrated directly. It is necessary to revert to laborious contour integration in the complex plane, which evaluates an integral of a function as the sum of the residues of the function, lying inside the path of integration. [35]

Finite Transforms. A special class of integral transforms arises when the range of the independent variable x is finite. The definition of a finite transform and its inverse are respectively:

$$T_x\big[f(x)\big] = \int_a^b f(x) \, K(\lambda, x) \, dx = F^x(\lambda) \tag{22}$$

$$T_x^{-1}\big[F^x(\lambda)\big] = \sum_{n=1}^\infty F^x(\lambda) K(\lambda_n, x) = f(x) \tag{23}$$

An important property of finite transforms can be observed from (23): the tedious contour integrals have been eliminated and the inverse is just an infinite series of orthogonal kernel functions.

Another important property of finite transformations is that the kernels are "tailored" to match the boundary conditions of the problem, making this method ideally suited to the solution of boundary value problems.

The limitations to this method are the following:

1. f (x) must satisfy Dirichlet's conditions in the interval (a,b), meaning, it must be piece-wise continuous and undergo bounded variation (same restrictions for uniform convergence of a Fourier series.)

2. This method will only solve those problems which have a Fourier Series solution. [40]

Initial Conditions. To demonstrate this method, the initial deformation of the disk due to rotation at a constant velocity will be determined by finite transforms. Reducing the system of equations (17) to a steady state problem gives:

$$
\left.
\begin{aligned}
&\bar{u}_{xx} + \tfrac{1}{x}\bar{u}_x - \tfrac{1}{x^2}\bar{u} = \tfrac{\rho}{E}a^2(1-\nu^2)\Omega^2(x+\bar{u}) \\
&\bar{u}(1) = 0 \\
&\bar{u}_x(\tfrac{b}{a}) + \tfrac{a}{b}\nu\,\bar{u}(\tfrac{b}{a}) = 0
\end{aligned}
\right\}
\tag{24}
$$

The $\bar{u}$ in the body force may be neglected, since $x \gg \bar{u}$.

From the definition of the transform (22), the transform of $\bar{u}$ is:

$$
T_{ux}[\bar{u}] = \int_1^{\tfrac{b}{a}} \bar{u}\, K(\lambda_n, x)\, dx = U^x(\lambda_n)
\tag{25}
$$

where the subscript ux indicated the x-transform is tailored to fit the $\bar{u}$ boundary conditions. Next all terms containing $\bar{u}$, or derivatives of $\bar{u}$ with respect to x, are collected and a transform is derived from (25) and the boundary conditions as follows:

let $D(\bar{u}) = \bar{u}_{xx} + \tfrac{1}{x}\bar{u}_x - \tfrac{1}{x^2}\bar{u}$

then $T_{ux}[D(\bar{u})] = \int_1^{\tfrac{b}{a}} D(\bar{u})\, K(\lambda_n, x)\, I(x)\, dx$

where I(x) is an integrating factor to facilitate integrating

by parts and is part of the kernel. In this case I (x) is found to be equal to x, letting the equation take the form:

$$T_{ux}\left[D(\bar{u})\right] = \int_{1}^{\frac{b}{a}} \left[(x\,\bar{u}')' - \frac{\bar{u}}{x}\right] K(\lambda_n, x)\, dx$$

where primes denote differentiation with respect to x.

Integration by parts twice yields:

$$T_{ux}\left[D(\bar{u})\right] = \left[K\,x\,\bar{u}' - K'\,x\,\bar{u}\right]_{1}^{\frac{b}{a}} + \int_{1}^{\frac{b}{a}} \left[(K'x)'\bar{u} - K\frac{\bar{u}}{x}\right] dx \qquad (26)$$

Assuming the transform of this operator can also be written.

$$T_{ux}\left[D(\bar{u})\right] = -\lambda_n^2 \int_{1}^{\frac{b}{a}} K\,x\,\bar{u}\, dx \qquad (27)$$

and choosing the boundary conditions on K (λ_n, x) such that the term in brackets preceeding the integral in (26) is equal to zero, makes it possible to equate the integrals in equations (26) and (27) to obtain the differential equation and the boundary conditions for K:

$$\left.\begin{aligned} (K'x)' - \frac{K}{x} + \lambda_n^2 K x &= 0 \\ K(1) &= 0 \\ K'(\tfrac{b}{a}) - \nu\,\tfrac{a}{b}\,K(\tfrac{b}{a}) &= 0 \end{aligned}\right\} \qquad (28)$$

It will be noted that this is a standard Sturm-Liouville system and has a Fourier series solution. [41] It is also valuable to note that the boundary conditions are identical to those of $\bar{u}$ and the equation is the same as $D(\bar{u}) = -\lambda^2\bar{u}$. The presence of the integrating factor does not change the solution of (28) as it may be divided out. These results can be generalized to other systems (called

"self-adjoint") as discussed in Churchill.[35]

The solution of (28) is:[37]

$$K(\lambda_n, x) = C_1 J_1(\lambda x) + C_2 Y_1(\lambda x)$$

where J_1 and Y_1 are Bessel functions of the first and second kinds of order one.

Using the first boundary condition, K (1)=0, to solve for the arbitrary constants gives $C_2 = -C_1 \frac{J_1(\lambda)}{Y_1(\lambda)}$ and the kernel function: (29)

$$K(\lambda_n, x) = C(\lambda)\left[Y_1(\lambda) J_1(\lambda x) - J_1(\lambda) Y_1(\lambda x)\right]$$

Transforms with this kernel function are known as "finite Hankle transforms."[40]

Applying the other boundary condition, it is found that $C(\lambda)$ divides out, therefore it is an arbitrary constant and can be taken (for convenience in inverse transformation) as a normalizing factor as defined by Wylie:[41]

$$C(\lambda) = \left[\frac{1}{2\lambda^2}\left[Y_1(\lambda) J_1(\lambda \tfrac{b}{a}) - J_1(\lambda) Y_1(\lambda \tfrac{b}{a})\right] - \frac{1}{\pi\lambda}\right]^{-\frac{1}{2}} \quad (30)$$

The second boundary condition gives the characteristic equation:

$$\frac{\lambda \tfrac{b}{a}}{1-\nu}\left[J_1(\lambda) Y_0(\lambda \tfrac{b}{a}) - Y_1(\lambda) - J_0(\lambda \tfrac{b}{a})\right]$$
$$= J_1(\lambda) Y_1(\lambda \tfrac{b}{a}) - Y_1(\lambda) J_1(\lambda \tfrac{b}{a}) \quad (31)$$

The values of λ which satisfy this equation are the eigenvalues and had to be determined numerically since the equacannot be solved for λ explicitly.

Applying the transform to the rest of equation (24), results in the following equation for U_0^x:

$$U_o^x = \frac{a^2 \omega_o^2}{\lambda^2 c_i^2} H_1(\lambda)$$

where $\quad c_i^2 = \frac{E}{\rho(1-\nu^2)}$ $\qquad$ (32)

and $\quad H_1(\lambda) = T_{ux} \, \chi \quad = \int_1^{\frac{b}{a}} K \, x^2 \, dx$

$$= C(\lambda) \int_1^{\frac{b}{a}} \left[Y_1(\lambda) \, J_1(\lambda x) - J_1(\lambda) Y(\lambda x) \right] x^2 \, dx \qquad (33)$$

which, by the bessel identities:

$$\int \chi^2 J_1(\alpha x) \, dx = \frac{\chi^2}{\alpha} \left[\frac{2}{\alpha x} J_1(\alpha x) - J_0(\alpha x) \right]$$

$$J_1(\alpha x) Y_2(\alpha x) - J_2(\alpha x) Y(\alpha x) = - \frac{2}{\pi \alpha x}$$

becomes:

$$H_1(\lambda_n) = C(\lambda) \left[Y_1(\lambda) \left[\frac{2}{\lambda^2} \frac{b}{a} J_1(\lambda \frac{b}{a}) - \frac{1}{\lambda} \left(\frac{b}{a}\right)^2 J_0(\lambda \frac{b}{a}) - \frac{2}{\lambda^2} J_1(\lambda) \right] \right.$$

$$\left. - J_1(\lambda) \left[\frac{2}{\lambda^2} \frac{b}{a} Y_1(\lambda \frac{b}{a}) - \frac{1}{\lambda} \left(\frac{b}{a}\right)^2 Y_0(\lambda \frac{b}{a}) - \frac{2}{\lambda^2} Y_1(\lambda) \right] \right]$$

Inverse Transform. Since the kernel forms an ortho-
normal set of functions with respect to the weight function x,
we may assume that $\bar{u}(x)$ may be expanded as an infinite
series of the form:

$$\bar{u}(x) = \sum_{n=1}^{\infty} a_n K(\lambda_n, x)$$

where a_n are arbitrary coefficients of the series.

Applying the principal of orthogonality to each term
in the series we get:

$$\int_1^{\frac{b}{a}} \bar{u} \, x \, K(\lambda_m, x) \, dx = \int_1^{\frac{b}{a}} a_n \, K(\lambda_n, x) K(\lambda_m, x) \, x \, dx$$

which equals zero except when $\lambda_n = \lambda_m$, hence:

$$a_n = \frac{\int_1^{\frac{b}{a}} \bar{u} \, x \, K(\lambda, x) \, dx}{\int_1^{\frac{b}{a}} K^2(\lambda, x) \, dx} \qquad (35)$$

The numerator of (35) is the definition of the

transform of $\bar{u}$ (22), while the denominator equals 1.0, since $K(\lambda, x)$ were normalized by $C(\lambda)$, therefore:

$$a_n = U_o^x$$

and the solution of the steady-state problem, which is the initial condition of the vibration problem, is:

$$\bar{u}(x) = \sum_{n=1}^{\infty} U_o^x K(\lambda_n, x) = \bar{u}_o \tag{36}$$

which agrees with inversion formula (23).

SOLUTION OF THE RADIAL DISPLACEMENT EQUATION

The solution of the radial displacement equation (19) can be obtained in the same manner after an examination of the terms in the body forces.

Transform of Body Forces. Assuming that a transform of equation (19) exists and taking the transform, we get:

$$-\lambda^2 U^x(\lambda, t) = \frac{a^2}{C_1^2}\left[U_{tt}^x(\lambda, t) - \Omega^2 H_1(\lambda) - \alpha V^x(\lambda, t) - 2\Omega V_t^x(\lambda, t) - \Omega^2 U^x(\lambda, t)\right]$$

Transforming the $\bar{v}$ equation, (20), produces a similar result:

$$-\beta^2 V^x(\beta, t) = \frac{a^2 \rho}{G}\left[V_{tt}^x(\beta, t) + \alpha H_2(\beta) + \alpha U^x(\beta, t) + 2\Omega U^x(\beta, t) - \Omega^2 V^x(\beta, t)\right]$$

Note that the transformed $\bar{u}$'s in the $\bar{u}$ equation are functions of λ, while the transformed $\bar{u}$'s in the $\bar{v}$ equation are functions of β. Therefore, they cannot be combined. Likewise for the $\bar{v}$'s, resulting in four unknowns in only two equations. Hence, no solution can be obtained unless the coupling terms in each equation can be neglected.

Order of Magnitude Consideration. The solution of a one-dimensional vibration problem by the method of separation

of variables assumes a Fourier series solution of the form:

$$u(x,t) = \sum X(x)\, T(t)$$

<div align="right">(37)</div>

where $X_n(x)$ is the mode shape or deflection curve and $T_n(t)$ is the time response, expressed as a trigonometric or exponential function of the natural frequencies. For a simple second order system $T(t)$ is usually of the form:

$$T(t) = A \cos \omega_n t + B \sin \omega_n t$$

where A and B are constants determined from the boundary conditions and ω_n is the natural frequency of the system in radians per second, obtained from the characteristic equation.

Now, consider the time derivatives of u:

$$u_t = \sum X(x)(\omega_n)(-A \sin \omega_n t + B \cos \omega_n t)$$

$$u_{tt} = \sum X(x)(-\omega_n^2)(A \cos \omega_n t + B \sin \omega_n t)$$

Therefore,

$$u_{tt} = O\left[\omega_n^2 u\right]$$
$$u_t = O\left[\omega_n u\right]$$
$$u = O\left[u\right]$$

Similar results are obtained for exponential functions. For systems with high natural frequencies, then:

$$u_{tt} \gg u_t \gg u$$

Likewise: $v_{tt} \gg v_t \gg v$

Similarly, if u_{tt} and v_{tt} are the same order of magnitude,

$$u_{tt} \gg v_t \gg v$$

$$v_{tt} \gg u_t \gg u$$

The solutions for $\bar{u}$ and $\bar{v}$ have the same form as (37),

the kernel function becoming the mode shape, $X(x)$, and the solutions of the ordinary differential equations in time, U^X and V^X, becoming the transient response, $T(t)$. Therefore, results similar to those of (38) are obtained, and the necessary assumptions can be made. This of course also assumes that Ω is not large enough to make $\Omega^2 \bar{u}$ of the same order of magnitude as $\bar{u}_{tt}$, which means that the natural frequency ω_n must be greater than Ω, such that: $\omega_n^2 >> \Omega^2$

If $\Omega = 0\left[\omega_n\right]$ then $\Omega^2 \bar{u} = O\left[\Omega\omega_n\bar{u}\right] = O\left[\omega_n^2\bar{u}\right]$, but all three terms are then negligible with respect to $\Omega^2 x$ and all but the $\Omega^2 x$ term can be omitted, which means the problem is no longer a vibration problem.

Neglecting all but $\bar{u}_{tt}$, $\bar{v}_{tt}$, $\Omega^2 x$ and $\propto x$ uncouples the equations, so that the vibrations in the radial and torsional modes can be considered as independent. The equation governing the radial or extensional vibrations becomes:

$$\bar{u}_{xx} + \frac{1}{x}\bar{u}_x - \frac{1}{x^2}\bar{u} = \frac{a^2}{c_i^2}\left[u_{tt} - \Omega^2 x\right] \tag{39}$$

X-Transform. Comparison of equations (39) and (24) made it apparent that the kernel functions of the transforms were identical, as also were $C(\lambda)$ and $H_1(\lambda)$. Therefore, the transform of the equation was straight forward and produced an ordinary differential equation in $\bar{u}$ and t:

$$U_{tt}^X + \lambda^2\frac{c_i^2}{a^2}U^X = \Omega^2 H_1(\lambda)$$

Note that in order to apply the initial conditions to this equation, they too had to be transformed with respect to X:

$$U^{''}(\lambda, 0) = \frac{a^2 \omega_o^2}{\lambda^2 c_1^2} H_1(\lambda) = U_o^x$$

$$U_t^x(\lambda, 0) = 0$$

<u>Laplace Transform</u>. Transforming this remaining equation by Laplace transforms gave the solution for U^{xt}:

$$Uxt = \frac{1}{S^2 + \frac{\lambda^2 c_1^2}{a^2}} \left[\frac{S a^2 \omega_o^2 H_1(\lambda)}{\lambda^2 c_1^2} + \overline{\Omega}^t(s) H_1(\lambda) \right]$$

where $\overline{\Omega}^t(s) = L_t \left[\Omega^2(t) \right]$

The inverse Laplace transform was:

$$U^x = \frac{a^2 \omega_o^2}{\lambda^2 c_1^2} H_1(\lambda) \cos \frac{\lambda c_1}{a} t + \frac{a}{\lambda c_1} H_1(\lambda) \int_0^t \Omega^2(\tau) \sin \frac{\lambda c_1}{a}(t - \tau) d\tau$$

Since $\Omega(t) = \omega_0 + \omega(t)$ then:

$$U^x = \frac{a^2 \omega_o^2}{\lambda^2 c_1^2} H_1(\lambda) + \frac{a}{\lambda c_1} H_1(\lambda) \int_0^t \left[\Omega^2(\tau) - \omega_o^2 \right] \sin \frac{\lambda c_1}{a}(t - \tau) d\tau$$

The first term in this equation is U_o^x, the steady-state solution already determined; the second term is the transient response due to the <u>change</u> in body force. $H_1(\lambda)$, it will be remembered, is the x-transform of x, so both terms have the form of $x \Omega^2$, but the second is also a type of periodic motion. This expression for U^x may be shortened to:

$$U^x = U_o^x + \frac{a}{\lambda c_1} H_1(\lambda) \xi(t) \tag{40}$$

where $\xi(t)$ represents the superposition integral.

The solution for $\bar{u}$ was, by the inverse transform theorem (23):

$$\bar{u}(x, t) = \sum_{n=1}^{\infty} U^x K(\lambda_n, x) \tag{41}$$

SOLUTION OF THE TANGENTIAL DISPLACEMENT EQUATION

Treating the $\bar{v}$ system of equations in a manner similar to the $\bar{u}$ system, that is, tailoring the kernel to match the system, the same differential equation for the kernel was obtained, but the boundary conditions differed, making the expressions for the normalizing factor and characteristic equation different. These results are listed below:

a) $\bar{v}$ equation and boundary conditions:

$$\bar{V}_{xx} + \frac{1}{x}\bar{V}_x - \frac{1}{x^2}\bar{V} = \frac{\rho a^2}{G}\left[\propto x + \bar{V}_{tt}\right]$$

$$\bar{V}(1,t) = 0 \qquad\qquad \bar{V}(x,0) = 0$$

$$\bar{V}_x\left(\frac{b}{a}\right) - \frac{a}{b}\bar{V}\left(\frac{b}{a}\right) = 0 \qquad \bar{V}_t(x,0) = 0$$

(42)

b) kernel function:

$$N(\beta_m, x) = D(\beta_m)\left[Y_1(\beta)J_1(\beta x) - J_1(\beta)Y_1(\beta x)\right]$$

(43)

c) Normalizing factor:

$$D(\beta_m) = \left[\frac{1}{2}\left(\frac{b}{a}\right)^2\left[Y_1(\beta)J_1\left(\beta\frac{b}{a}\right) - J_1(\beta)Y_1\left(\beta\frac{b}{a}\right)\right]^2 - \frac{1}{\pi\beta}\right]^{-\frac{1}{2}}$$

(44)

d) Characteristic equation:

$$\frac{\beta a}{2b}\left[J_1(\beta)Y_0\left(\beta\frac{b}{a}\right) - Y_1(\beta)J_0\left(\beta\frac{b}{a}\right)\right] = J_1(\beta)Y_1\left(\beta\frac{b}{a}\right) - Y_1(\beta)J_1\left(\beta\frac{b}{a}\right)$$

(45)

Solution by Transforms. The x-transform of the equation resulted in the differential equation:

$$V_{tt}^x + \frac{\beta^2 c_2^2}{a^2}V^x = -\propto(t)H_2(\beta)$$

where: $c_2^2 = \frac{G}{\rho}$

$$H_2(\beta) = D(\beta)\left[Y_1(\beta)\left[\frac{2}{\beta^2}\frac{b}{a}J_1\left(\beta\frac{b}{a}\right) - \frac{1}{\beta}\left(\frac{b}{a}\right)^2 J_0\left(\beta\frac{b}{a}\right) - \frac{2}{\beta^2}J_1(\beta)\right]\right.$$

$$\left. - J_1(\beta)\left[\frac{2}{\beta^2}\frac{b}{a}Y_1\left(\beta\frac{b}{a}\right) - \frac{1}{\beta}\left(\frac{b}{a}\right)^2 Y_0\left(\beta\frac{b}{a}\right) - \frac{2}{\beta^2}Y_1(\beta)\right]\right]$$

(46)
(47)

The reader will notice the striking similarities in the foregoing and corresponding expressions from the $\bar{u}$ solution.

Laplace transform:

$$V^{xt} = -\frac{H_2(\beta)\,\bar{\alpha}^t(s)}{s^2 + \frac{\beta^2 c_2^2}{\alpha^2}}$$

where: $\bar{\alpha}^t(s) = L_t\left[\alpha(t)\right]$

Inverse Laplace transform:

$$V^x = -\frac{\alpha}{\beta c_2} H_2(\beta) \int_0^t \alpha(\tau)\, \mathcal{L}\!-\!(t-\tau)\,d\tau \qquad (48)$$

$$= -\frac{\alpha}{\beta c_2} H_2(\beta)\, \eta(t)$$

where $\eta(t)$ equals the superposition integral.

The inverse X-transform:

$$\bar{V}(x,t) = \sum_{m=1}^{\infty} N(\beta_m, x) V^x(\beta_m, t) \qquad (49)$$

STRESS AND STRAIN SOLUTIONS

Equations (6) and (7) showed the stresses and strains in terms of displacements, therefore, substituting the solutions for $\bar{u}$ and $\bar{v}$ results in a known series expansion for the stresses and strains in terms of the free vibration modes and transient response terms. The non-dimensionalized forms of (6) and (7) are:

$$\left.\begin{aligned}
\bar{\sigma}_x &= \sigma_x\,\frac{1-\nu^2}{E} = \frac{\partial \bar{u}}{\partial x} + \nu\,\frac{\bar{u}}{x} \\[4pt]
\bar{\sigma}_\theta &= \sigma_\theta\,\frac{1-\nu^2}{E} = \frac{\bar{u}}{x} + \nu\,\frac{\partial \bar{u}}{\partial x} \\[4pt]
\bar{\tau}_{r\theta} &= \frac{\tau_{r\theta}}{G} = \frac{\partial \bar{v}}{\partial x} - \frac{\bar{v}}{x}
\end{aligned}\right\} \qquad (50)$$

$$\left.\begin{aligned}
\epsilon_r &= \frac{\partial \bar{u}}{\partial x} \\[4pt]
\epsilon_\theta &= \frac{\bar{u}}{x} \\[4pt]
\gamma_{r\theta} &= \frac{\partial \bar{v}}{\partial x} - \frac{\bar{v}}{x}
\end{aligned}\right\} \qquad (51)$$

Since the same four terms occur in all six express-
ions, it is necessary to evaluate only the following:

$$\frac{\overline{U}}{X} = \sum_{n=1}^{\infty} \frac{C(\lambda)}{X}\left[Y_1(\lambda)J_1(\lambda x) - J_1(\lambda)Y_1(\lambda x)\right]U^x(\lambda,t)$$

$$\frac{\partial \overline{u}}{\partial X} = \sum_{n=1}^{\infty} \lambda_n\, C(\lambda)\left[Y_1(\lambda)\left(J_0(\lambda x) - \frac{J_1(\lambda x)}{\lambda x}\right)\right.$$
$$\left. - J_1(\lambda)\left(Y_0(\lambda x) - \frac{Y_1(\lambda x)}{\lambda x}\right)\right]U^x(\lambda,t)$$

$$\frac{\overline{V}}{X} = \sum_{m=1}^{\infty} \frac{D(\beta)}{X}\left[Y_1(\beta)J_1(\beta x) - J_1(\beta)Y_1(\beta x)\right]V^x(\beta,t)$$

$$\frac{\partial \overline{V}}{\partial X} = \sum_{m=1}^{\infty} \beta_m\, D(\beta_m)\left[Y_1(\beta)\left(J_0(\beta x) - \frac{J_1(\beta x)}{\beta x}\right)\right.$$
$$\left. - J_1(\beta)\left(Y_0(\beta x) - \frac{Y_1(\beta x)}{\beta x}\right)\right]V^x(\beta,t)$$

(52)

Substituting numerical results for these four series
into equations (50) and (51) will give solutions for both
the stresses and the strains.

IV. FREE VIBRATION AND TRANSIENT RESPONSE

NUMERICAL RESULTS

<u>Natural Frequencies</u>. The natural frequencies of the disk in free vibration appeared in the transformed equations, (40) and (48). The natural frequencies in radians per second for the extensional vibration were determined to be:

$$\omega_n = \frac{\lambda_n c_1}{a} = \frac{\lambda_n}{a} \sqrt{\frac{E}{\rho(1-\nu^2)}}, \quad (n=1,2,3....) \tag{53}$$

and for torsional vibration:

$$\omega_m = \frac{\beta_m c_2}{a} = \frac{\beta_m}{a} \sqrt{\frac{G}{\rho}}, \quad (m=1,2,3,....) \tag{54}$$

Two sets of non-dimensional frequencies were then defined as:

$$\left. \begin{aligned} \lambda_n &= \frac{\omega_n a}{c_1} \\ \\ \beta_m &= \frac{\omega_m a}{c_2} \end{aligned} \right\} \tag{55}$$

These, it will be noticed, are simply the eigenvalues of equations (31) and (45), the characteristic equations from the $\bar{u}$ and $\bar{v}$ solutions. For this reason, the characteristic equations are often termed the "frequency equations" in vibration problems. An examination of these equations reveals that λ_n depends upon the geometry of the disk and Poisson's ratio of the material, while β_m depends upon the geometry only.

The quantities c_1 and c_2 are respectively, the two-

dimensional propagation velocities of the dilatational and distortional stress waves in solids. The dilatational wave is a compression wave in the material characterized by particle motion in the direction of propagation. [34, 39]

To demonstrate the effect of the physical properties of materials on these velocities, the approximate values in inches per second are listed below for steel and for a photoelastic rubber to be mentioned in Chapter V:

	c_1	c_2
Carbon steel	$217 \times 10^3 \frac{in.}{sec}$	$123 \times 10^3 \frac{in.}{sec}$
Photoelastic rubber [33]	$2.63 \times 10^3 \frac{in.}{sec}$	$1.37 \times 10^3 \frac{in.}{sec}$

Numerical Data. Before the series solutions of Chapter III can be evaluated, the roots or eigenvalues of the characteristic equations must be found. In general, it is necessary to determine only the first few roots, since the terms of the converging series steadily decrease in magnitude and soon make very little contribution to the result.

Numerical results were obtained for the roots of the frequency equations for the first five natural frequencies, where possible, and for integral ratios of b/a from 2.0 to 15.0. The extensional eigenvalues were calculated for ν values of 0.3 and 0.5 to show that the effect of Poisson's ratio was slight. The results are plotted on graphs, Figs. 2, 3, and 4, and tabulated to four decimals in Appendix A. A comparison of values on the graphs shows that the only
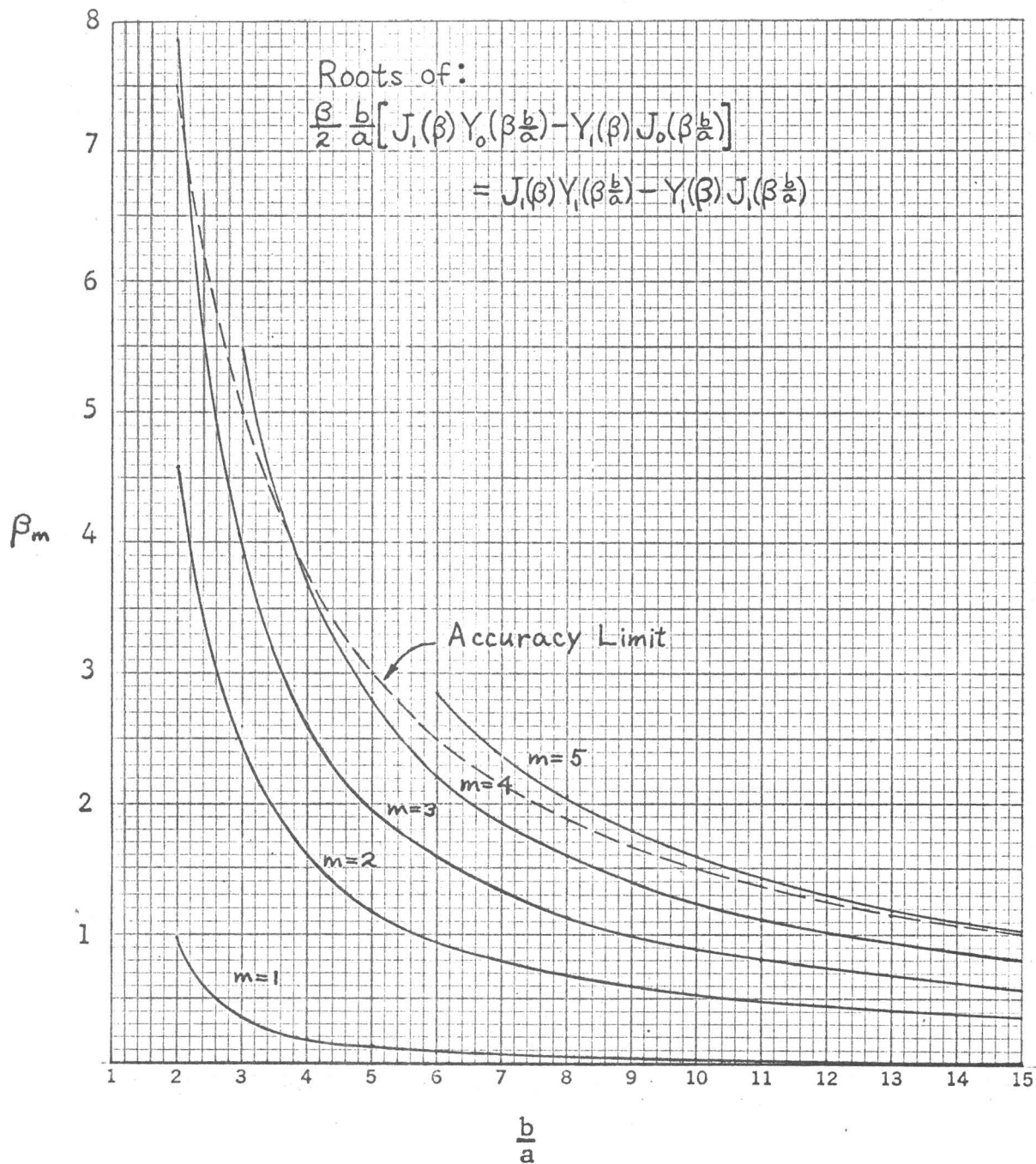
Figure 2. Eigenvalues for the free torsional vibration of a uniform annular disk versus the radii ratio.
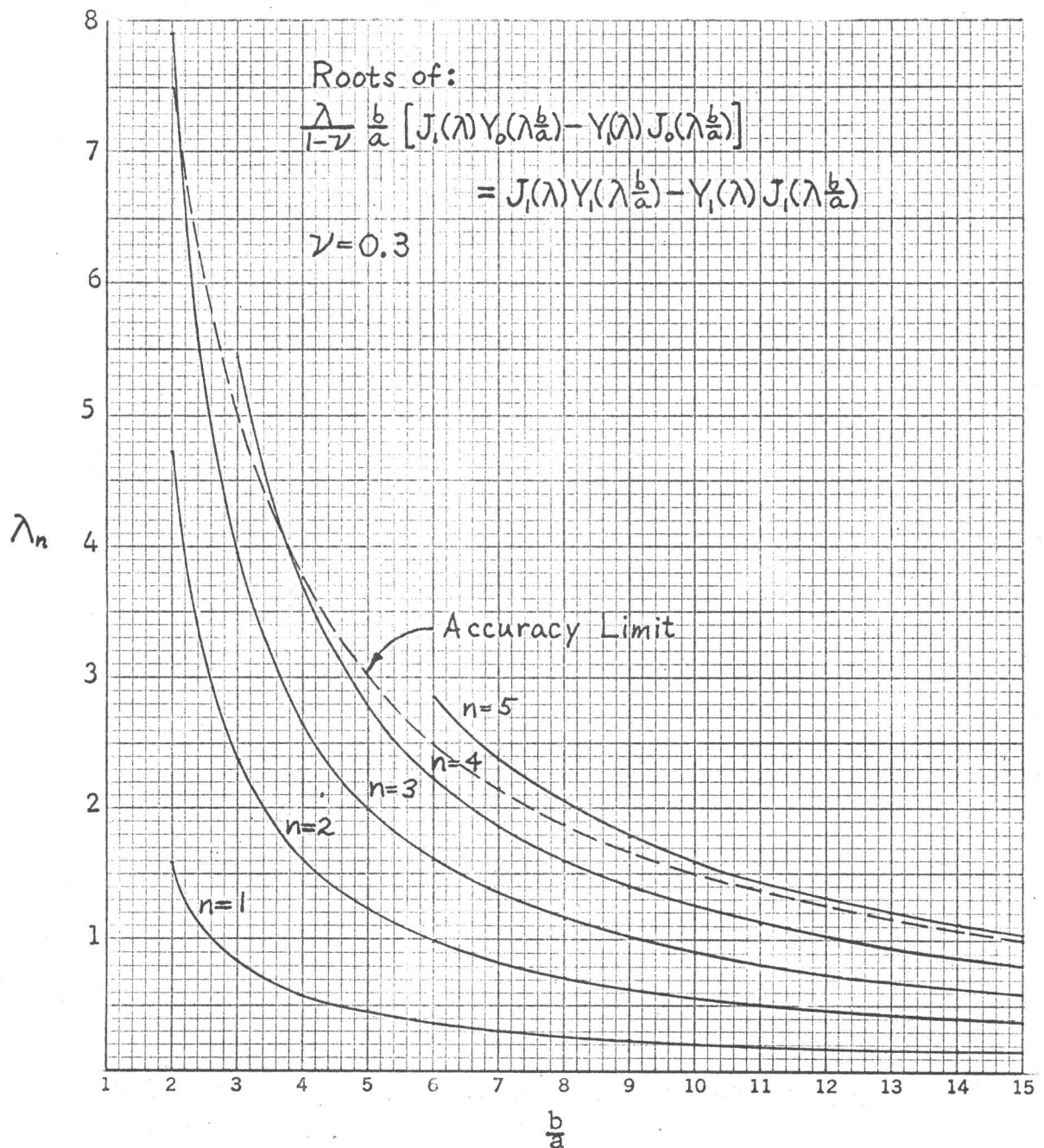
Figure 3. Eigenvalues for the free extensional vibration of a uniform annular disk versus the radii ratio. Poisson's ratio: $\nu = 0.3$
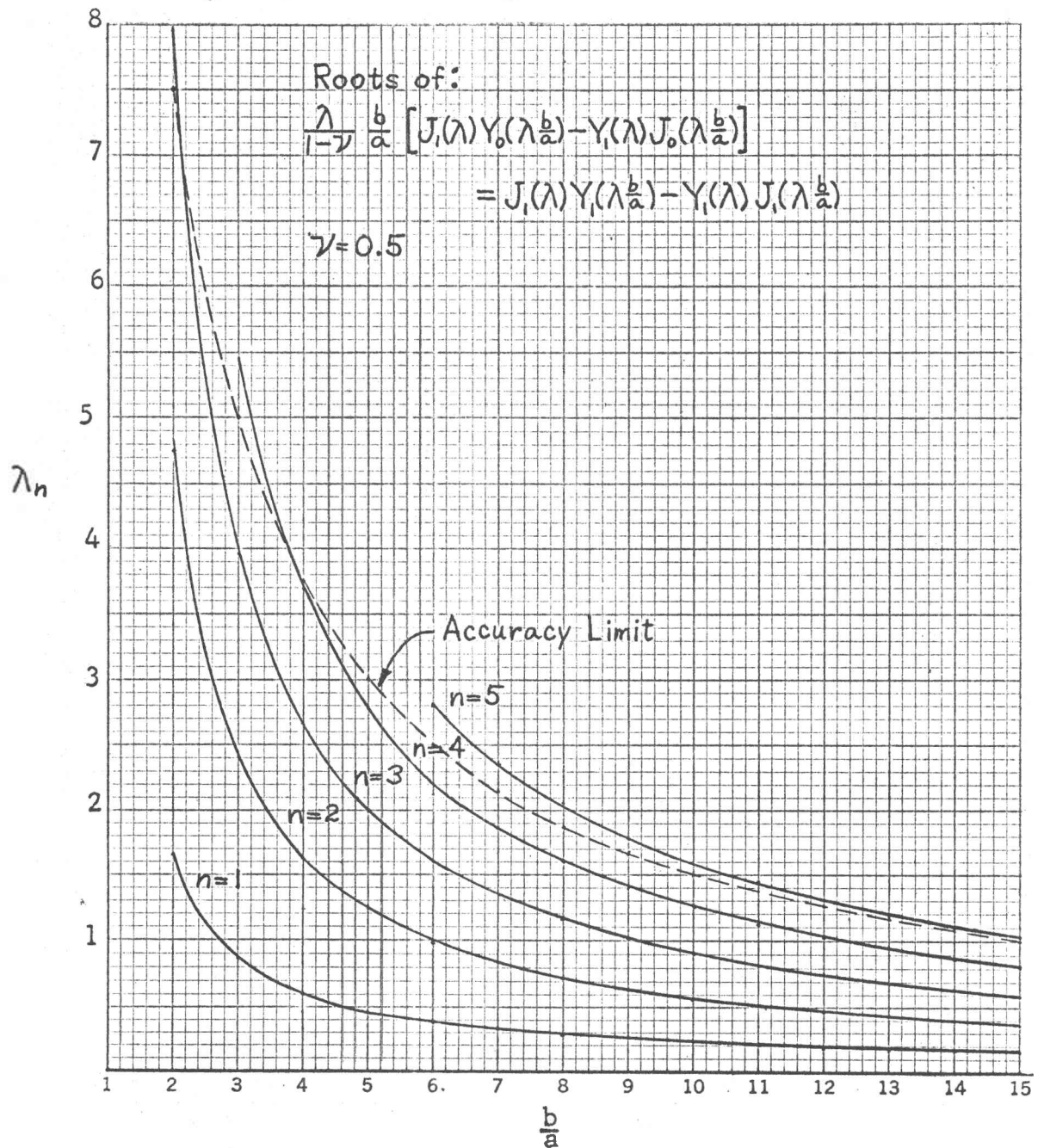
Figure 4. Eigenvalues for the free extensional vibration
of a uniform annular disk versus the radii ratio.
Poisson' ratio: $\nu = 0.5$

significant difference in λ_n and β_m occurred between the very first frequency or fundamental mode of the two types of vibration. The first three frequencies of each mode were found to agree, within normal limits of accuracy, with Simmonds' results, [22], thus helping to substantiate his solution over that of Singh and Nandeeswaraiya. [23]

The mode shapes for torsonal vibration are plotted graphically in Fig. 5(a) to (e). They represent the shape or deflection curve of a radial line of the disk at its maximum deformation. The amplitudes are plotted to an exaggerated scale on rectangular coordinates. For small deflections, the displacements can be considered nearly normal to an undeformed radial line. Each higher mode of vibration has a decreased amplitude, illustrating convergence, and one additional node, or non-oscillating point of the disk. These nodes form concentric circles of torsionally stationary points. The mode shapes for the extensional vibrations have been plotted in Fig. 6 (a) to (e), only the displacements had to be plotted normal to a radial line, rather than in their true radial direction, for the sake of visibility. Similar nodal circles were found, only these were stationary with respect to radial displacement.

The radii of the nodal circles have been calculated numerically for each of the eigenvalues. Each set of nodes is listed next to its corresponding eigenvalue in Tables II, III, and IV of Appendix A. In Fig. 7, the nodes have been plotted for the third mode of extensional vibration.
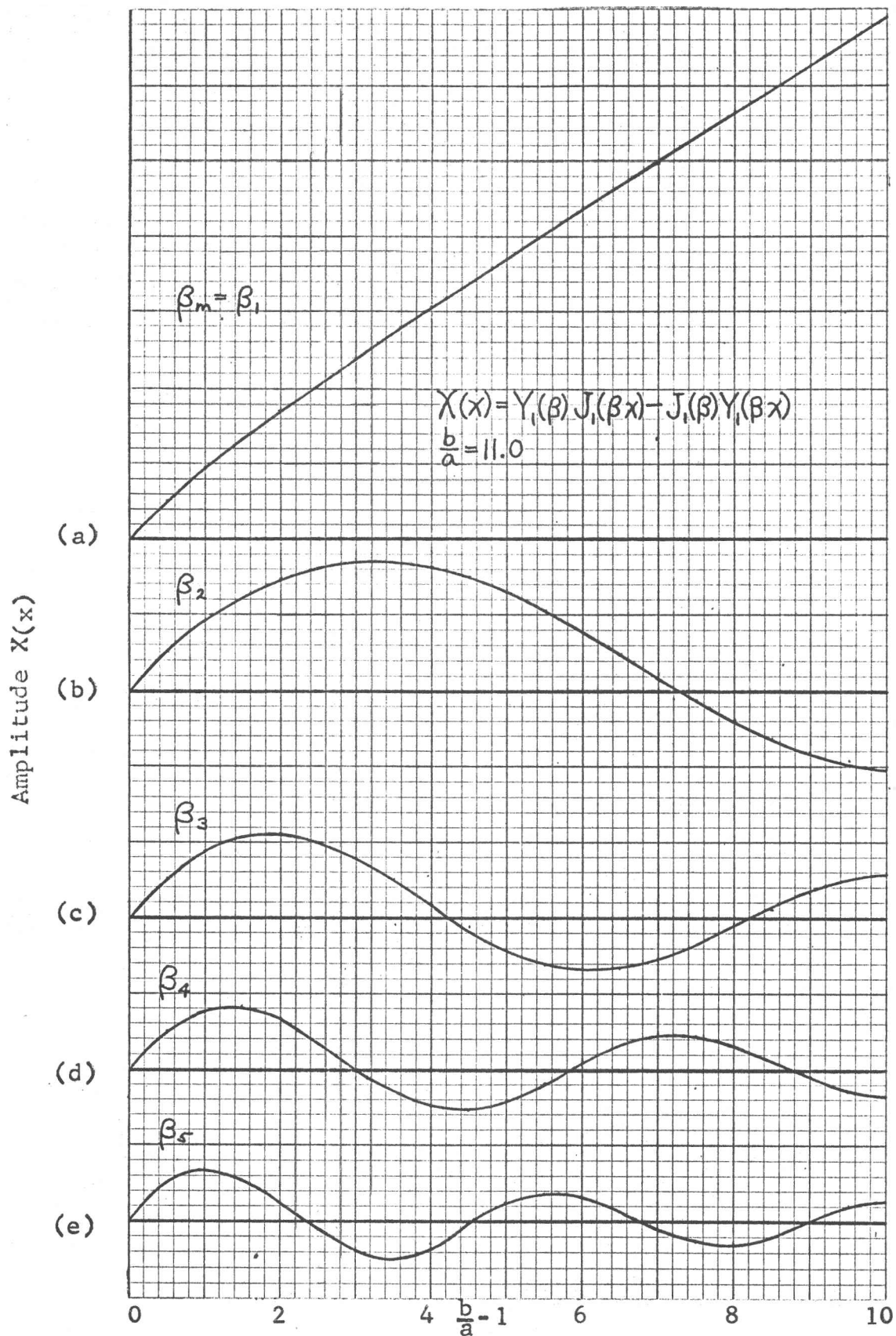
Figure 5. Qualitative mode shapes of the first five natural frequencies of torsional vibration for a uniform annular disk.
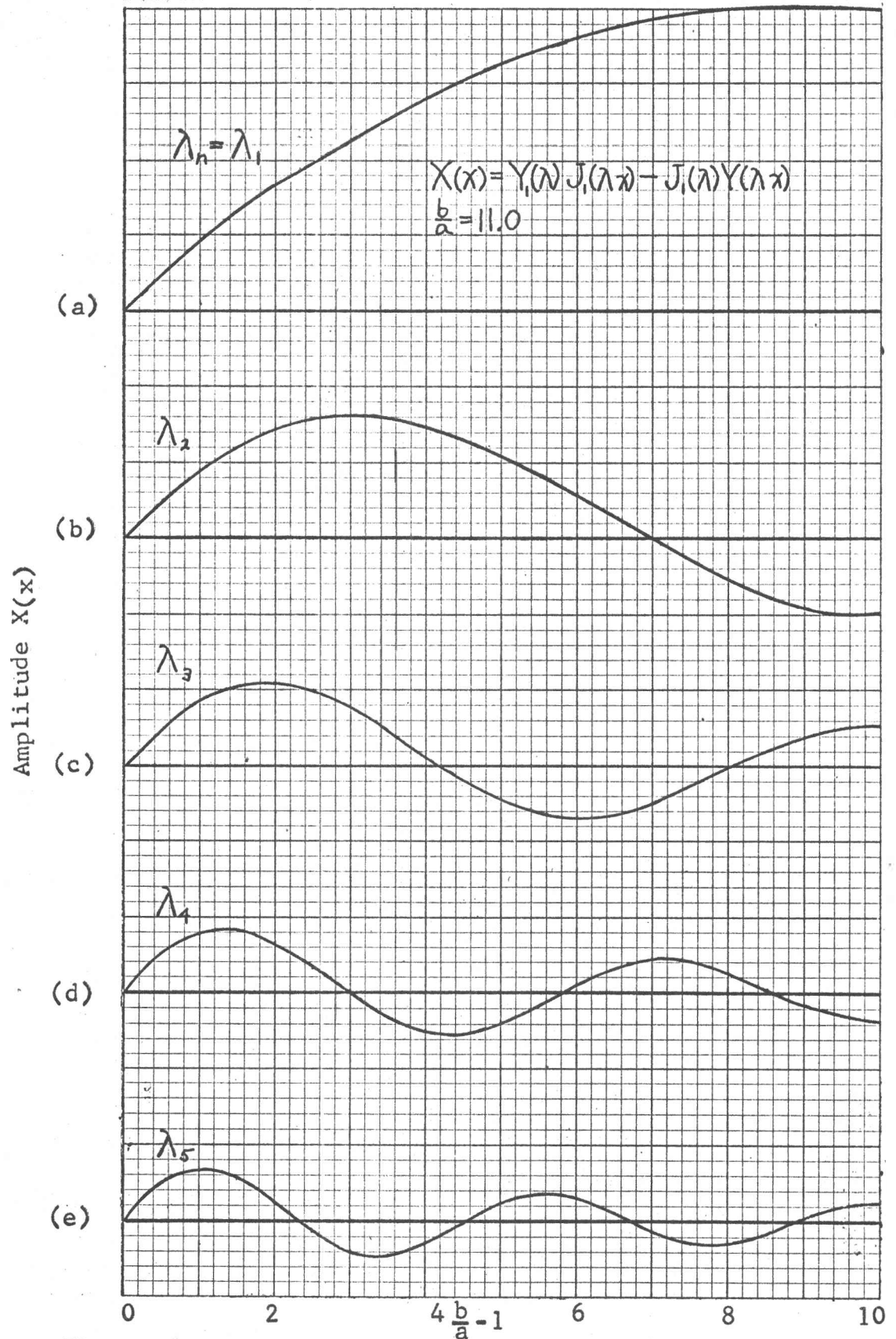
Figure 6. Qualitative mode shapes of the first five natural frequencies of torsional vibration for a uniform annular disk.
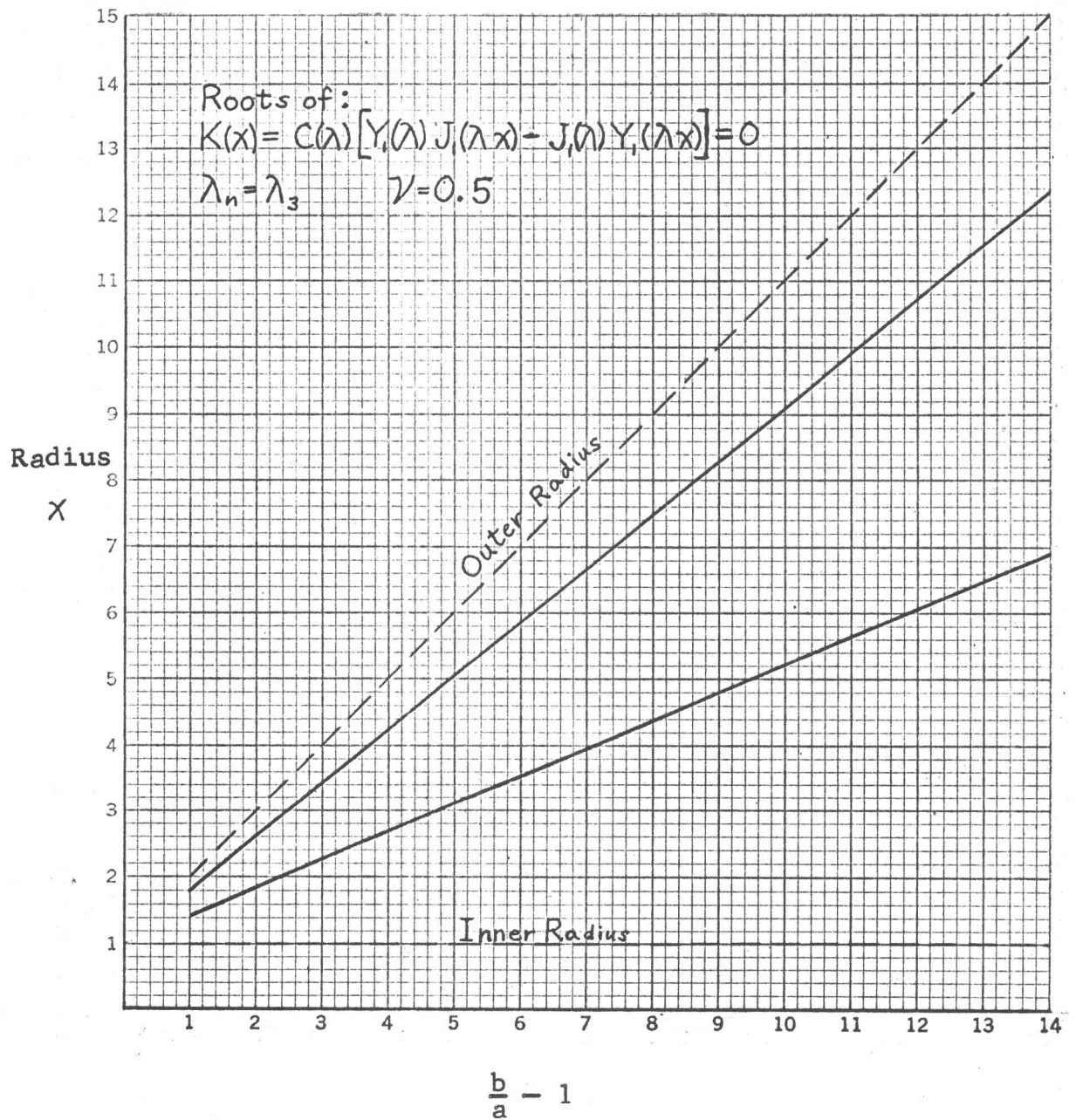
Figure 7. Nodal radii versus $\frac{b}{a} - 1$ for the third mode of extensional vibration of a uniform annular disk. Poisson's ratio: $\nu = 0.5$

This plot indicates that the nodes vary proportionally with the size of the disk. When plotted versus $\frac{b}{a}$ -1. they divide each size disk into the same proportions.

For close approximations, the constant of proportionality can be determined from the nodes of $\frac{b}{a}$-1 equal to 10.0. By subtracting 1.0 from these nodal radii and multiplying the remaining number by 10.0, the percentage of the distance from 1 to b/a is obtained and can be used in determining the nodes for other b/a values, even non-integral values. Results obtained by this method, for the extensional mode shown in Fig. 7, were compared to the actual percentages for b/a equal to 4.0 and 15.0. They were found to differ by no more than 1.12% and by as little as 0.18%.

Empirical Formulas for Frequencies. The analysis of the nodal circles with respect to $\frac{b}{a}$-1 led to the discovery of empirical formulas representing the natural frequency curves of Figs. 2,3, and 4. When plotted on logarithmic coordinates versus $\frac{b}{a}$-1, as in Fig. 8, the frequency curves became linear, indicating a relationship of the form:

$$\log \lambda_n = m_n \log\left(\frac{b}{a}-1\right) + \log B_n$$

$$\text{or} \quad \lambda_n = B_n\left(\frac{b}{a}-1\right)^{m_n}$$

(56)

where m_n is the slope of the line. Both m_n and B_n are constants that differ for each mode of vibration and, for the extensional vibrations, they differ for each ν value. Values for m_n, B_n and $\log B_n$ were determined by the method of least-squares and are found in Table I for each mode of vibration
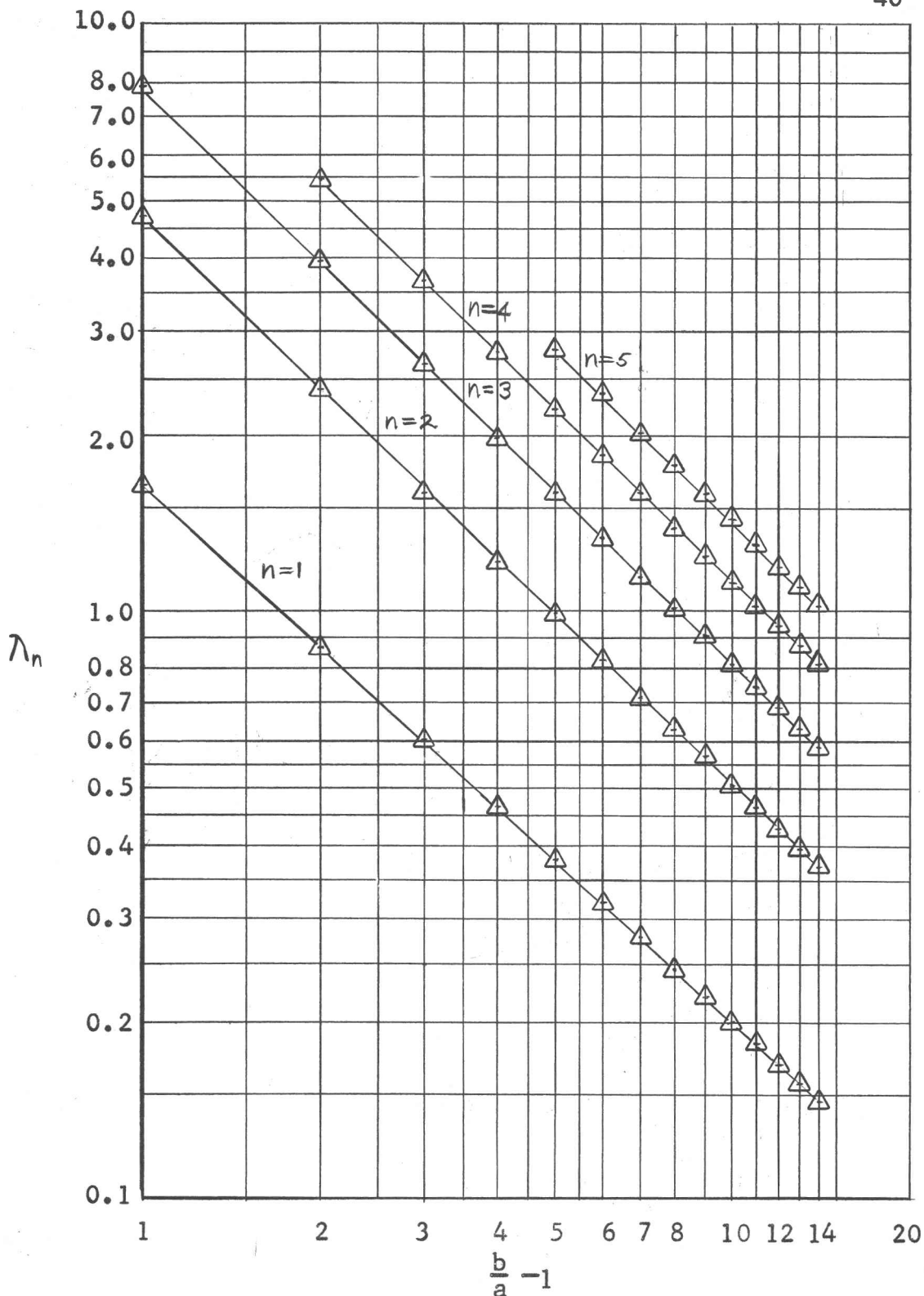
Figure 8. Logarithmic plot of eigenvalues for the free extensional vibrations of a uniform annular disk to determine empirical relationship with radii ratio. Poisson's ratio: $\nu = 0.5$

TABLE I

SLOPE AND INTERCEPT OF EMPIRICAL NATURAL FREQUENCY
EQUATIONS FOR TORSIONAL AND EXTENSIONAL
VIBRATIONS OF A UNIFORM ANNULAR DISK.

Mode	Slope	Intercept	$\log_{10}$ of Intercept	Correlation Coefficient
n	m_n	B_n	$\log_{10} B_n$	r_{xy}
Torsional Modes				
1	-1.6712007	1.1286800	.052570857	-.99896819
2	-.97334013	4.5249686	.65561557	-.99996903
3	-.98724215	7.7489946	.88924536	-.99997489
4	-.98838096	10.828437	1.0345658	-.99999636
5	-.99254082	14.034957	1.1472111	-.99994853
Extensional Modes: ν =0.3				
1	-.92391975	1.5872712	.20065114	-.99999095
2	-.96741117	4.6839973	.67061664	-.99998578
3	-.98387661	7.8302141	.89377364	-.99998577
4	-.98329493	10.807996	1.0337452	-.99999335
5	-.98673173	13.916854	1.1435411	-.99997020
Extensional Modes: ν =0.5				
1	-.91858087	1.6580299	.21959236	-.99998603
2	-.96658420	4.7078827	.67282564	-.99998763
3	-.98476765	7.8660153	.89575479	-.99997823
4	-.98319931	10.821343	1.0342812	-.99999306
5	-.98036740	13.675001	1.1359274	-.99987867

and for $\mathcal{V}$ values of 0.3 and 0.5.

The maximum deviation from the linearized curves occured at the lowest mode of torsional frequencies. Correlation coefficients, r_{xy}, were determined for each linear equation and are also found in Table I. This coefficient is a measure of how well the straight lines represent the data. Ideally it should equal ± 1.0. It is evident from an examination of Table I that there was very little scatter of the data about the line. Even the first torsional mode had an r_{xy} of-0.99896819.

These empirical relations should be invaluable for design work and will also simplify the numerical solutions to be obtained in the experimental phase of this project. They are particularly useful in determining the natural frequencies for fractional values of $\frac{b}{a}$, and in extrapolating for values beyond the range of the tables. When carried to the limit, they indicate an infinite frequency for $\frac{b}{a}=0$ and a frequency of zero for $\frac{b}{a}=\infty$, which agrees with the approximations proposed by Simmonds. [22]

Discussion of Error. All of the Bessel functions in the frequency and mode shape equations were calculated to the nearest 0.00001 from their infinite series definitions, while the eigenvalues and nodes were found by iterative techniques to the nearest 0.0005. All calculations were made at the Brigham Young University Computer Research Center on an IBM 650 digital computer. Although the calculations were made to eight significant figures, the results have

been rounded off to four, corresponding to their required accuracy.

The Bessel function subroutines used were limited in accuracy to an argument (x or λx) of 15.0, therefore, the highest value of λ or β which could be computed accurately was $\frac{b}{a}\lambda < 15$ or $\frac{b}{a}\beta < 15$. At arguments near 15, the dominant $J_n(x)$ in each calculation was found to be between 0.25 and 1.0% in error, while the dominant $Y_n(x)$ was from 0.25 to 4.0% in error, making a maximum probable error of 5% in the combined functions in equations (29),(31),(43),(45).

The equations cited above all have a similar form-- the difference of products of Bessel functions. On sampling the change in magnitude of the function for a small change in argument x, the ratio was found to be as high as 1259:1. This means that λ and β are not very sensitive to errors in the Bessel functions. However, this steepness of slope introduced considerable error into iteration process, sometimes causing more than one value to be found for the same eigenvalue. An accuracy limit line has been plotted on the frequency curves, Figs 2,3,and 4, indicating the argument $\lambda\frac{b}{a}$ or $\beta\frac{b}{a}$ equal to 15.0. Values near this curve are to be used with a lesser degree of confidence.

RESPONSE TO SPECIFIED INPUTS

The response of the disk to a general shaft input has been expressed in terms of superposition or Duhamel's integrals. To determine the response of the system to any

specific input function, then, it is only necessary to evaluate the following two integrals, since the rest of the solution remains the same:

$$\xi(t) = \int_0^t \left[\Omega^2(\tau) - \omega_o^2 \right] \sin \omega_n(t-\tau) d\tau \qquad (57)$$

$$\eta(t) = \int_0^t \alpha(\tau) \sin \omega_m(t-\tau) d\tau$$

To assist in evaluating the integrals, a number of simple superposition intergals were evaluated and they are listed in Table V of Appendix B. The three input functions that follow were selected as the best approximations of physically realizable inputs that were still comparatively simple.

Step-Change in Velocity. For the simple case of a step-change in shaft velocity, the shaft inputs become:

$$\Omega(t) = \omega_o \qquad t < 0$$
$$= \omega_o + \omega_s \qquad t \geq 0$$

where ω_o is the initial velocity and ω_s is the magnitude of the step change, and:

$$\alpha(t) = 0 \qquad t < 0$$
$$= \delta(t) \qquad t = 0$$
$$= 0 \qquad t > 0$$

where $\delta(t)$ is a unit impulse or delta function, that is, a pulse of infinite amplitude and zero time duration. The integrals for this case are:

$$\xi(t) = \int_0^t (2\omega_o \omega_s + \omega_s^2) \sin \omega_n(t-\tau) d\tau$$

by (a), Appendix B:

$$= \frac{1}{\omega_n} (2\omega_o \omega_s + \omega_s^2)(1 - \cos \omega_n t) \qquad (58)$$

$$\eta(t)= \int_0^t \delta(t) \sin \omega_n(t-\tau) d\tau$$

by (a), Appendix B:

$$= \frac{1}{\omega_m}(1-\cos \omega_m t)$$

(59)

<u>Sinusoidal Shaft Input</u>. For a sinusoidal shaft input:

$$\Omega(t) = \omega_0 + \omega_s \sin \omega_1 t$$

$$\alpha(t) = \omega_s \omega_1 \cos \omega_1 t$$

where ω_s is the magnitude of the sine wave and ω_1 is its frequency. The integrals for this case become:

$$\xi(t)= \int_0^t (2 \omega_0 \omega_s \sin \omega_1 \tau + \omega_s^2 \sin \omega_1 \tau) \sin \omega_n(t-\tau) d\tau$$

by (g) and (d), Appendix B:

$$= 2\omega_0\omega_s \left(\frac{\omega_1 \sin \omega_n t - \omega_n \cos \omega_1 t}{\omega_1^2 - \omega_n^2}\right) - \frac{\omega_s^2}{2\omega_n}(1-\cos \omega_n t)$$

$$+ \frac{\omega_s^2 \omega_n}{2(4\omega_1^2 - \omega_n^2)}(\cos 2\omega_1 t - \cos \omega_n t)$$

(60)

$$\eta(t)= \int_0^t \omega_s \omega_1 \cos \omega_1 \tau \sin \omega_m(t-\tau) d\tau$$

by (f), Appendix B:

$$= \omega_s \omega_1 (\cos \omega_1 t - \cos \omega_m t) \frac{\omega_m}{\omega_1^2 - \omega_m^2}$$

(61)

<u>Combined Sine-Ramp-Step Function</u>. For this function:

$$\Omega(t) = \omega_0 + \frac{\omega_s}{T_1}\left(t - \frac{1}{\omega_1}\sin \omega_1 t\right) \qquad 0 \le t \le T_1$$

$$= \omega_0 + \omega_s \qquad\qquad t > T_1$$

$$\alpha(t) = \frac{\omega_s}{T_1}(1-\cos \omega_1 t) \qquad 0 \le t \le T_1$$

$$= 0 \qquad\qquad t > T_1$$

The intergrals then become, for the interval $0 \le t \le T_1$:

$$\xi(t)= \int_0^t \left[\frac{2\omega_0 \omega_s}{T_1}\left(\tau - \frac{1}{\omega_1}\sin \omega_1 \tau\right)\cdot \right.$$

$$\left. + \frac{\omega_s^2}{T_1^2}\left(\tau^2 - \frac{2\pi}{\omega_1}\sin \omega_1 \tau + \frac{1}{\omega_1^2}\sin^2 \omega_1 \tau\right)\right] \sin \omega_n(t-\tau) d\tau$$

by (b),(c),(d),(e),(g) and remembering that $\omega_1 T_1 = 2\pi$:

$$
\begin{aligned}
\xi(t) = & \frac{2\omega_0\omega_s}{T_1\omega_n^2}(\omega_n - \sin\omega_n t) - \frac{\omega_0\omega_s}{\pi}\left(\frac{\omega_1\sin\omega_n t - \omega_n\sin\omega_1 t}{\omega_1^2 - \omega_n^2}\right) \\
& + \frac{\omega_s^2}{T_1^2}\left[\frac{t^2}{\omega_n} - \frac{2}{\omega_n^3}(1 - \cos\omega_n t)\right] \\
& - \frac{\omega_s^2}{\pi T_1}\left[\frac{T}{2}\left(\frac{\omega_1\sin\omega_n t - \omega_n\sin\omega_1 t}{\omega_1^2 - \omega_n^2}\right) - \frac{\omega_1^2 + \omega_n^2}{(\omega_1^2 - \omega_n^2)^2}(\cos\omega_1 t - \cos\omega_n t)\right] \\
& + \frac{\omega_s^2}{8\pi^2}\left[\frac{1 - \cos\omega_n t}{\omega_n} + \frac{\omega_n}{4\omega_1^2 - \omega_n^2}(\cos 2\omega_1 t - \cos\omega_n t)\right]
\end{aligned}
\tag{62}
$$

$$
\eta(t) = \int_0^t \frac{\omega_s}{T_1}(1 - \cos\omega_1 T)\sin\omega_m(t - T)\, dT
$$

by (a) and (f): Appendix B:

$$
= \frac{\omega_s}{T_1\omega_m}(1 - \cos\omega_m t) - \frac{\omega_s\omega_m}{T_1}\left(\frac{\cos\omega_m t - \cos\omega_1 t}{\omega_1^2 - \omega_m^2}\right)
\tag{63}
$$

For the interval $t > T_1$ we must return to the Laplace transform solutions of Chapter III. The solutions for U^{xt} and V^{xt}, before substituting initial conditions are:

$$
U^{xt} = \frac{1}{s^2 + \omega_n^2}\left[s\, U^x(T_1) + U_t^x(T_1) + \overline{\Omega}^t(s)H_1(\lambda)\right]
$$

$$
V^{xt} = \frac{1}{s^2 + \omega_n^2}\left[s\, V^x(T_1) + V_t^x(T_1) - \overline{\alpha}^t(s)H_2(\beta)\right]
$$

where $U^x(T_1)$, $V^x(T_1)$, etc, are the conditions at the start of the interval, evaluated from the solution for the interval $0 \le t \le T_1$:

$$
\begin{aligned}
U^x(T_1) = & \frac{\omega_0^2}{\omega_n^2}H_1(\lambda) + \frac{H_1(\lambda)}{\omega_n}\left[\frac{2\omega_0\omega_s}{\omega_n^2 T_1}(\omega_n - \sin\omega_n T_1)\right. \\
& - \frac{\omega_0\omega_s}{\pi}\left(\frac{\omega_1\sin\omega_n T_1}{\omega_1^2 - \omega_n^2}\right) + \frac{\omega_s^2}{\omega_n} - \frac{2}{T_1}\frac{\omega_s^2}{\omega_n^3}(1 - \cos\omega_n T_1) \\
& - \frac{\omega_s^2}{\pi T_1}\left[\frac{T_1}{2}\frac{\omega_1\sin\omega_n T_1}{\omega_1^2 - \omega_n^2} - (1 - \cos\omega_n T_1)\frac{(\omega_1^2 + \omega_n^2)}{(\omega_1^2 - \omega_n^2)^2}\right] \\
& \left. + \frac{\omega_s^2}{8\pi^2}\left[\frac{1 - \cos\omega_n T_1}{\omega_n} + \frac{\omega_n}{4\omega_1^2 - \omega_n^2}(1 - \cos\omega_n T_1)\right]\right]
\end{aligned}
$$

$$U^X(T_1) = \frac{\omega_0^2}{\omega_n^2} H_1(\lambda) + \frac{H_1(\lambda)}{\omega_n} \xi(T_1)$$

$$U_t^X(T_1) = \frac{H_1(\lambda)}{\omega_n} \left[\frac{2\omega_0\omega_s}{\omega_n T_1}(-\cos \omega_n T_1) - \frac{\omega_0\omega_s\omega_1\omega_n}{\pi(\omega_1^2 - \omega_n^2)}(\cos \omega_n T_1 - 1) \right.$$

$$+ \frac{\omega_s^2}{T_1^2}\left(\frac{2T_1}{\omega_n} - \frac{2}{\omega_n^2} \sin \omega_n T_1\right) - \frac{\omega_s^2}{2\pi T_1}\left[\frac{\omega_1 \sin \omega_n T_1}{\omega_1^2 - \omega_n^2}\right]$$

$$+ \frac{2\pi \omega_n}{\omega_1^2 - \omega_n^2}(\cos \omega_n T_1 - 1)\right] + \frac{\omega_s^2}{\pi T_1}\frac{(\omega_1^2 + \omega_n^2)}{(\omega_1^2 - \omega_n^2)^2}(\sin \omega_n T_1)$$

$$+ \frac{\omega_s^2}{8\pi^2}\left(\sin \omega_n T_1 + \frac{\omega_n^2 \sin \omega_n T_1}{4\omega_1^2 - \omega_n^2}\right) \Bigg]$$

$$= \frac{H_1(\lambda)}{\omega_n} \xi_t(t)$$

$$V^X(T_1) = -\left[\frac{H_2(\beta)}{\omega_m^2} \frac{\omega_s}{T_1}(1 - \cos \omega_m T_1) - \frac{\omega_s}{T_1} \omega_m^2 \frac{\cos \omega_m T_1 - 1}{\omega_1^2 - \omega_n^2}\right]$$

$$= -\frac{H_2(\beta)}{\omega_m} \eta(T_1)$$

$$V_t^X(T_1) = -H_2(\beta)\left[\sin \omega_m T_1 + \frac{\omega_s}{T_1}\frac{\omega_m \sin \omega_m T_1}{\omega_1^2 - \omega_m^2}\right]$$

$$= -\frac{H_2(\beta)}{\omega_m} \eta_t(T_1)$$

And the solution for $t > T_1$ becomes:

$$U^X = U^X(T_1)\cos \omega_n t + \frac{U_t^X(T_1)}{\omega_n}\sin \omega_n t$$

$$\left. + \frac{H_1(\lambda)}{\omega_n^2}(2\omega_0\omega_s + \omega_s^2)(1 - \cos \omega_n t) \atop V^X = V^X(T_1)\cos \omega_m t + \frac{V_t^X(T_1)}{\omega_m}\sin \omega_m t \atop - \frac{H_2(\beta)}{\omega_m^2}(1 - \cos \omega_m t) \right\} \quad (64)$$

These solutions for three different cases contain both the transient response, in terms of the natural frequencies, and the steady-state response, in terms of the forcing function parameters. In the latter two cases, singularities occur when the frequency of the forcing function is equal to a natural frequency or sometimes one half of a natural frequency. This was expected, since no structural or other damping was considered.

V. PRELUDE TO THE EXPERIMENTAL INVESTIGATION

CURRENT EXPERIMENTAL TECHNIQUES

Dynamic Photoelasticity. The problem of the tran-
sient response of a rotating disk seems ideally suited to
experimental investigation by dynamic photoelasticity, a
technique used increasingly in the study of wave propagation
and transient stresses. Goldsmith [31] cites the advantages
of this method as: (1) a complete stress picture of the
entire field can be obtained rather than few finite points,
and (2) the measurements are accomplished with light and,
therefore, they add no mass to the experimental model and
do not alter its response. He further cites the disadvan-
tages as: (1) the model materials are significantly diff-
erent in physical properties from the engineering materials
they represent, (2) the materials require accurate dynamic
calibration, and (3) additional information is needed be-
fore individual stresses may be determined at interior
points. (points not on a free boundary). Consequently,
photoelastic investigations of transient phenomena often
requires reliable independent measurements or an appropriate
theory as a check on the results obtained.

Photoelastic materials are viscoelastic, that is
they will creep when subjected to a constant load. Gold-
smith states [31] that most transient phenomena are of too
short a duration to be affected by the creep of the material,

but the viscous effects do increase the dissipation of energy and dispersion of stress waves. They also cause some of the physical properties, such as the modulus of elasticity, to be dependent upon the rate of loading, hence the problem of dynamic calibration. The calibration of the material must be made at the same loading rate as the model experiences. Dynamic calibration has successfully been accomplished by using a vibrating beam for a photoelastic model. [27,30]

Low Modulus Materials. Stress waves ordinarily propagate at such high velocities that it requires very high speed photography to stop the motion. Recently, a technique has been developed based on the fact that propagation velocities in a material are a function of the modulus of elasticity of the material. Utilizing low-modulus materials, propagation velocities have been reduced to the neighborhood of 2000 inches per second (see the first section of Chapter IV). Successful movies with a rotating-prism framing camera have recorded transient events at framing rates as low as 6,000 frames per second. [26,29,32,33] This is the technique that is recommended for the experimental phase of this study.

The Photoelastic Method. The instrument of photoelastic analysis, the polariscope, employs a beam of polarized light to produce an interference pattern consisting of dark and light bands or fringes on the optical image of a model. Each band represents the locus of points on the model

that have the same magnitude of the difference in principal
stresses, the magnitude depending on the order of the band
and the constant of proportionality of the birefringent
model material. Numerous methods have been devised to
provide an additional relationship, so that the photoelastic
data may be separated into individual stresses. [27] Some of
the techniques require independent measurements at finite
points; others require an approximation by finite defferences;
still others require a repetition of the test, so a second
interference pattern can be obtained, differing from the
first by a known relationship. The first group of proced-
ures is not considered acceptable as it is usually inadequate
and difficult to obtain in transient problems, the second
group is long and tedious, but the third is acceptable if
the events are repeatable. Two of the latter group are men-
tioned here as possible techniques to be utilized in the
experimental phase of this analysis. They are the "oblique
incidence" and "interferometer" methods.

Oblique Incidence. The oblique incidence method is
simply a variation of the ordinary polariscope technique.
Ordinarily, the photoelastic model is two-dimensional and is
viewed with the model normal to the transmitted light. By
the oblique incidence method, the model is inclined at an
angle to the incident light, thus producing a second
fringe pattern. The use of this method and the relationship
between the two fringe patterns is discussed by Drucker. [28]
He states that it is limited to thin models with low stress

gradients, since the polarized light enters and leaves the model at different locations that must not have widely differing stress magnitudes.

Interferometry. An interferometer is an optical instrument which divides a beam of parallel light, by means of a half-silvered mirror called a "beam-splitter," into two separate beams, initially in phase. When used for stress analysis, one beam is passed through a loaded model, the other through an unloaded model, then the two beams are reunited by another beam-splitter and an interference effect results. The stresses in the model alter its thickness because of the Poisson's ratio of the material, effectively changing the path length of one light beam. This may result, at some points, with the beam becoming out of phase with its unaltered twin, thus producing a pattern of light and dark bands or fringes that are proportional to the varying model thickness. It can be shown that the change in thickness of a two dimensional model is proportional to the sum of the principal stresses, consequently each band of the interference pattern corresponds to the locus of points on the model having the same magnitude of principal stress sum, the magnitude depending on the order of the band and the constant of proportionality of the model material. This, along with the photoelastic fringe pattern, provides two equations in terms of the principal stresses, which can be solved simultaneously for individual stresses at any point on the model. A number of variations of this instrument have been used and

are described in refrence [27].

GENERAL CONSIDERATIONS AND RECOMMENDATIONS

Repeatability. The principal disadvantage of the
experimental techniques discussed in the preceding sections,
when used in the analysis of transients, is the necessity
of repeating the event in order to obtain information in
support of the photoelastic data. It does not seem probable
that the results of any two tests would be identical in both
time and magnitude.

Considering this problem, two systems are proposed
as possible solutions, each making possible the simultan-
eous determination of two independent sets of data during a
single test of a model. The first combines an oblique and
a normal incidence polariscope into one instrument; the
second combines a polariscope and an interferometer into a
single instrument.

It is theorized that combining a normal and oblique
incidence polariscope can be accomplished by dividing the
incident light into two beams, as illustrated on Fig. 9,
passing one through the model normally and the other
obliquely, then reuniting them for photographing simultan-
eously. Suitable shields are placed in the light paths so
that only opposite halves of each beam are allowed to pass
through the model to the camera. This limits the method to
the investigation of systems of stresses that possess a
line of symmetry. The field of view would be divided about
the line of symmetry, one side displaying the normal
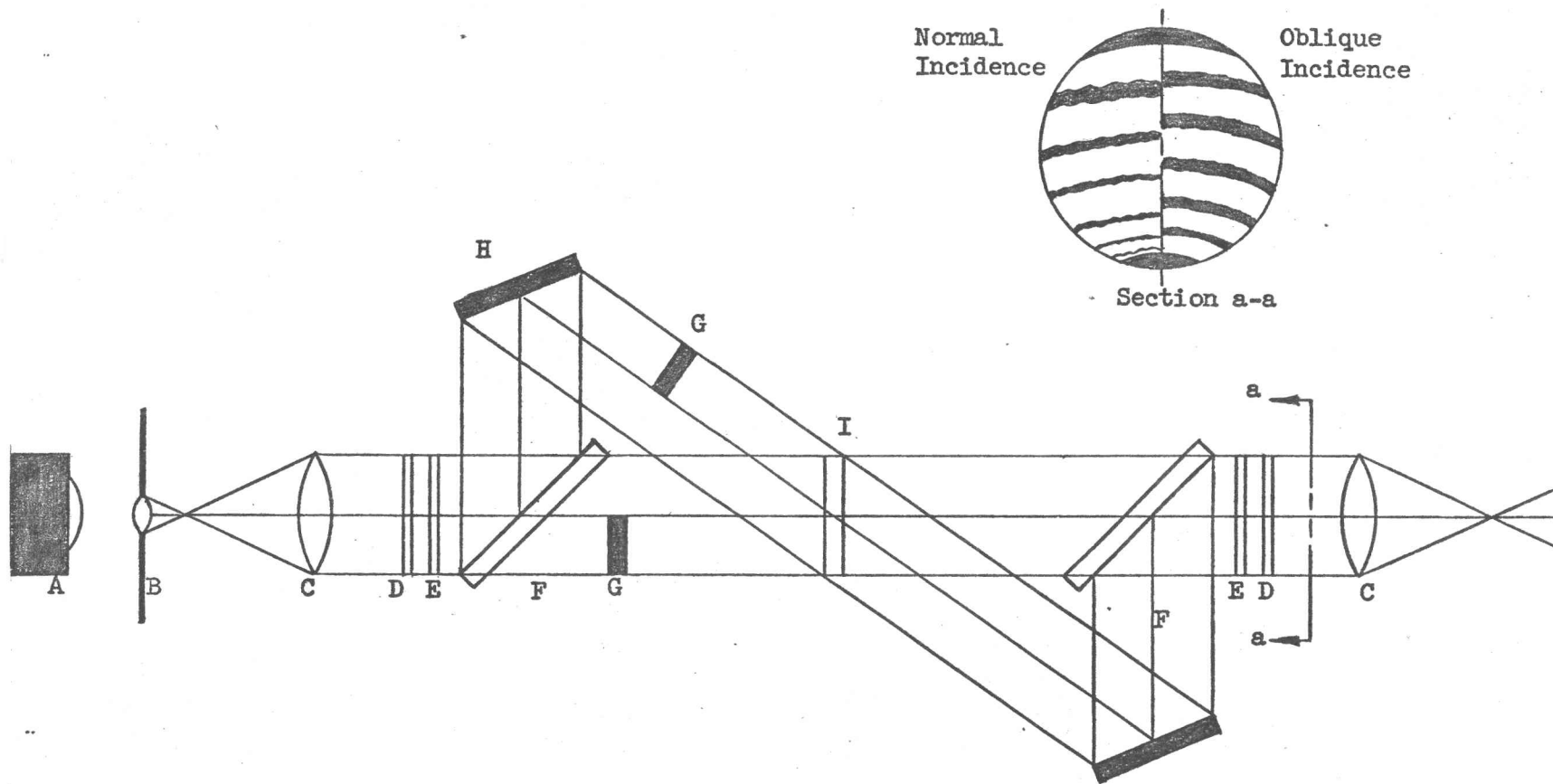
Figure 9. Schematic of a Combined Normal and Oblique Incidence Polariscope

A – Light source   E – Quarter-wave plate   I – Model
B – Aperture   F – Half-silvered mirror
C – Lens   G – Opaque screen
D – Polarizing plate   H – Plane mirror

incidence fringe pattern, the other the oblique, as depicted in the inset of Fig. 9. Certainly, the beam splitters form- ing the oblique system could be replaced by full-silvered mirrors covering only half the field of view, providing the edges of the mirrors were sufficiently accurate.

The combination of a polariscope and interferometer could be accomplished in a similar manner, as illustrated in Fig. 10. Since the light beam is already split in an inter- ferometer, the portion which is passed through the model could be divided in two about a line of stress symmetry, as previously described, and polarizing plates inserted in one half to form a polariscope. The same limitations as to stress symmetry are necessarily applicable to this system.

These systems are not without difficulties, but other than allignment problems, it is believed that no serious difficulties in addition to those existing in separate systems would be introduced.

The most serious difficulties to surmount arise from the extreme sensitivity of the interferometer, which must adhere to tolerances as fine as one quarter of a wave length of light. The first of these is: the instrument must be carefully isolated from all sources of vibration, which is complicated by the fact that the model itself is required to vibrate. The second is the required accuracy of the model surface. Previous investigators have found it necessary to polish the surface of the model to the quality of an optical flat, [27] , thus limiting the investigations to very small
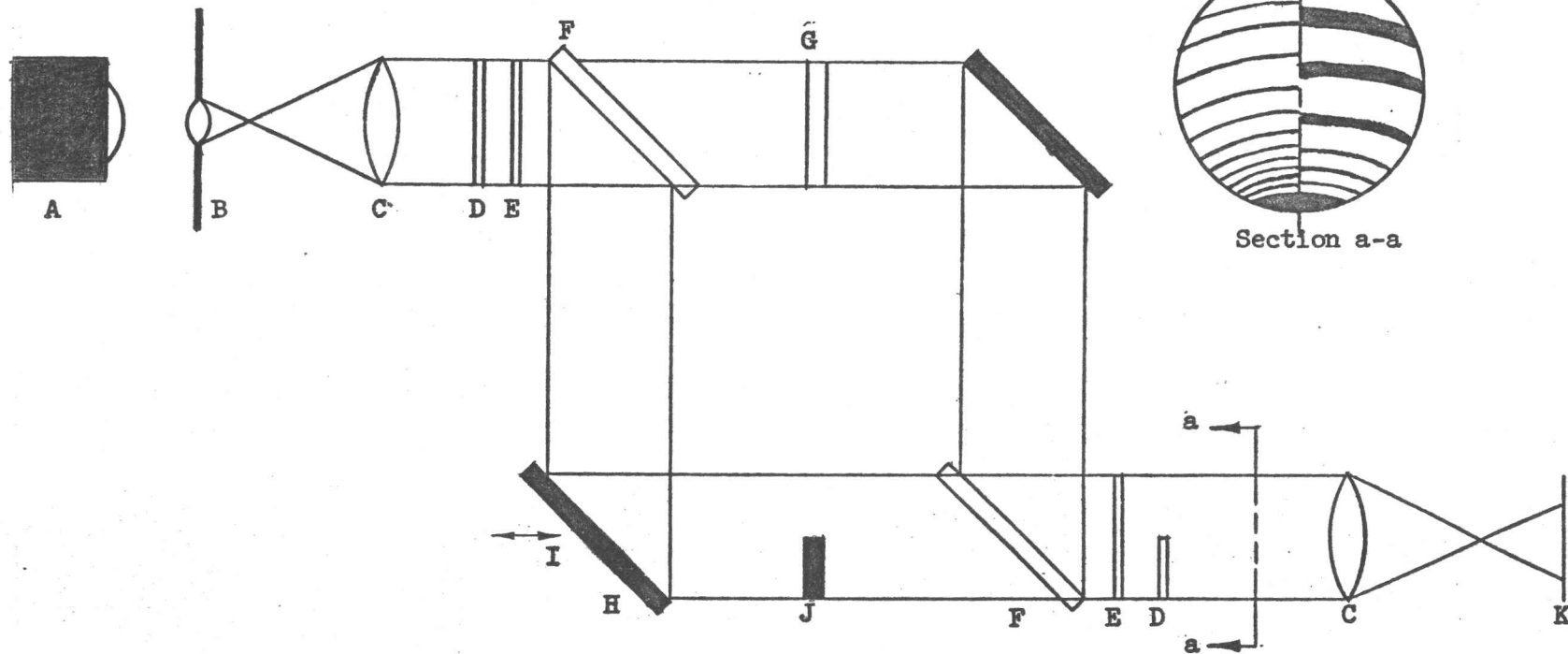
Figure 10. Schematic of Combined Polariscope and Interferometer

A - Light source
B - Aperture
C - Lens
D - Polarizing Plate
E - Quarter-wave plate

F - Half-silvered mirror
G - Model
H - Plane Mirror
I - Micro-micro path length
    adjustment

J - Opaque screen
K - Image

models. Unfortunately, the present low-modulus materials
often have residual stresses or non-homogeneities that
would produce fringes in an unstressed model even though
the flat surfaces were perfectly parallel. A possible
solution might be to take a "tare reading", a photograph of
the interference fringes of the unloaded model, which could
then be subtracted from subsequent fringe patterns to obtain
the absolute magnitude of stresses. The periphery of the
disk would have to be marked with a code, so that the lo-
cation of the stresses could be identified and the proper
correction applied.

Dynamic Similarity. The concept of dynamic similar-
ity makes possible the generalization of experimental results.
To achieve dynamic similarity, the governing differential
equations must be non-dimensionalized with respect to all
independent variables, and the resulting coefficients made
equal for corresponding coefficients of the prototype and
the model. In the analysis contained in Chapter II, the
equations were non-dimensionalized with respect to the geo-
metric variables only. For complete similarity, the time
variable and input functions must also be made dimensionless
with respect to some characteristic value of the system hav-
ing the dimensions of time.

In the differential equation for $\bar{u}$, Equation(39),
the time dependent terms $\bar{u}_{tt}$ and $\Omega^2(t)X$, both have the
units of $1/sec^2$. If ω_o is chosen as the non-dimensionaliz-
ing parameter, both terms can be non-dimensionalized by

dividing by ω_0^2 . This, of course, must be compensated by an ω_0^2 in the coefficient, making the equation become:

$$\bar{u}_{XX} + \frac{1}{X}\bar{u}_X - \frac{1}{X^2}\bar{u} = F_s\left[\bar{u}_{TT} - \Omega^2(T)X\right] \tag{65}$$

where T denotes non-dimensional time, $\omega_0 t$, and F_s is a dimensionless dynamic similitude parameter equal to:

$$F_s = \frac{\rho(1-\nu^2)a^2\omega_0^2}{E} = \frac{a^2\omega_0^2}{c_1^2} \tag{66}$$

As a natural consequence to the solution of equation (65), the natural frequencies appear in the non-dimensional form:

$$\bar{\omega}_n = \frac{\omega_n}{\omega_0} = \frac{\lambda_n c_1}{a\,\omega_0} = \frac{\lambda_n}{\sqrt{F_s}} \tag{67}$$

Similarly, non-dimensionalizing the $\bar{v}$ equation,(42) results in the dynamic similitude parameter:

$$C_s = \frac{\rho}{G}a^2\omega_0^2 \tag{68}$$

and the dimensionless natural frequency :

$$\bar{\omega}_m = \frac{\omega_m}{\omega_0} = \frac{\beta_m c_2}{a\,\omega_0} = \frac{\beta_m}{\sqrt{C_s}} \tag{69}$$

A model which is dynamically similar to its prototype must therefore have a and ω_0 adjusted so that its F_s and C_s parameters, along with the dimensionaless inputs,

$$\frac{\Omega^2(t)}{\omega_0^2} \quad \text{and} \quad \frac{\alpha(t)}{\omega_0^2}$$

are equal to like parameters for the prototype. Then all measurements must be non-dimensionalized to correspond to the dimensionless coordinates $\frac{r}{a}$ and $\omega_0 t$ and dimensionless variables $\frac{u}{a}$ and $\frac{v}{a}$.

<u>Loading Apparatus</u>. The design of an apparatus to produce impulsive shaft inputs will require the utmost of ingenuity. Such problems as the finite time required before an actuator takes affect, bouncing and chatter between members brought into contact, and flexibility of the loading members must be minimized by careful design.

A possible choice of a sinusoidal input device for the case of a sine wave superimposed on a constant shaft velocity, would be a u-joint drive turned at a small angle to the drive shaft. This closely approximates the given function.

<u>Model Size</u>. The model should be kept as large as possible, so that as many pictures as possible may be obtained before the dilatation wave is reflected off the outer boundary. On the other hand, the extreme flexibility of the model material requires that it be as small as possible to minimize transverse motion, which would introduce unwanted bending stresses. Hence, a compromise will have to be made. It may be found necessary to use smaller models and a faster camera.

Other points worthy of consideration are:

1. <u>Thickness coupling</u>. The low modulus materials have low natural frequencies. It will be necessary to keep the frequencies of forcing functions low and the disk thin in comparison to its radius to avoid the coupling effects of the thickness.

2. <u>Increasing shutter speed</u>. The effective speed of the camera can be increased by a flashing or modulated light source, synchronized with the framing of the camera. This, however, would not alter the time between frames, but would stop the motion better than the framing of the camera alone.

3. <u>Eccentricity and balancing</u>. The disk must be balanced within close tolerances, so that the conditions of axially symmetric loading are met.

4. <u>Test of methods</u>. It would be wise to verify the accuracy of the methods used by first determining the stresses in a disk rotating with a constant velocity, since this solution has been verified by other means.

With the techniques thus verified, they may be extended to numerous complex applications, such as examining the response of rotating members with:

1. eccentric shafts

2. flexible hubs

3. discontinuities

4. peripheral excitation

5. jerk or acceleration gradients

6. forcing frequency near a natural frequency

7. shock loaded peripheral gear teeth

VI SUMMARY

In the foregoing chapters, an analysis has been made of the in-plane vibrations of a uniform disk with a concentric hole. Finite Hankel transforms have been used to obtain a series solution of the approximate equations of motion for the radial and tangential displacements, derived from plane stress theory. It was concluded that finite transforms could not be applied to coupled equations. Fortunately, it was also determined that the coupling terms, such as the coriolis acceleration terms, could be omitted, as their effect on the over-all stresses and displacements was negligible. General solutions were obtained in terms of superposition integrals containing general functions for the shaft inputs, so that any integrable function could be chosen.

To facilitate numerical solutions of the series expressions for the stresses and displacements, three simple input functions were selected and the superposition integrals evaluated. Also, the first five natural frequencies for each mode of vibration were determined numerically, so that the first five terms of each series solution could be evaluated. Should the plane stress theory give inadequate results, a correction factor may be applied to the natural frequencies, such as the one proposed by Mosely. [7]

Useful empirical relations were discovered, relating the natural frequencies to the geometry of the disk by a linear logarithmic equation. A linear relation was also found between the nodes of vibration and the geometry of the disk. These relations were found to be highly accurate and should prove valuable in design work. The results should provide sufficient information for the determination of numerical solutions, which can be used to verify the experimental data.

Two-dimensionless parameters were introduced, making possible the generalization of experimental results to rotating disks of any elastic material.

APPENDIX

APPENDIX A

TABLE II

EIGENVALUES AND NODES FOR THE TORSIONAL MODES OF FREE VIBRATION OF A UNIFORM ANNULAR DISK.

Diam. Ratio $\frac{b}{a}$	Mode m	Eigen-values β_m	Nodes	Diam. Ratio $\frac{b}{a}$	Mode m	Eigen-values β_m	Nodes
2.0	1	.9869		7.0	1	.05959	
	2	4.5891	1.6918		2	.7877	5.3213
	3	7.8545	1.4020		3	1.3159	3.5122
			1.8036				5.9234
3.0	1	.3627			4	1.8395	2.7695
	2	2.2973	2.4051				4.4921
	3	3.8940	1.8176				6.2065
			2.6287		5	2.3720	2.3594
	4	5.4763	1.5781				3.6938
			2.1240				5.0220
			2.7280				6.3601
4.0	1	.1916		8.0	1	.04514	
	2	1.5419	3.1275		2	.6790	6.0586
	3	2.6038	2.2349		3	1.1316	3.9453
			3.4497				6.7512
	4	3.6563	1.8719		4	1.5803	3.0733
			2.7355				5.0798
			3.5976				7.0754
5.0	1	.1194			5	2.0449	2.5853
	2	1.1653	3.8555				4.1341
	3	1.9598	2.6566				5.6758
			4.1732				7.2171
	4	2.7472	2.1684	9.0	1	.03577	
			3.3196		2	.5972	6.7965
			4.4674		3	.9931	4.3805
6	1	.08147					7.5790
	2	.9388	4.5879		4	1.3850	3.3809
	3	1.5738	3.0825				5.6716
			5.0977				7.9490
	4	2.2022	2.4678		5	1.7859	2.8250
			3.9058				4.5993
			5.3374				6.3647
	5	2.8250	2.1353				8.1355
			3.2549				
			4.3701				
			5.5025				

TABLE II (CONTINUED)

Diam. Ratio	Mode	Eigen-values	Nodes	Diam. Ratio	Mode	Eigen-values	Nodes
$\frac{b}{a}$	m	β_m		$\frac{b}{a}$	m	β_m	
10.0	1	.02873		13.0	1	.01694	
	2	.5333	7.5360		2	.4044	9.7589
	3	.8851	4.8175		3	.6688	6.1404
			8.4070				10.8952
	4	1.2338	3.6886		4	.9297	4.6249
			6.2616				8.0423
			8.8189				11.4374
	5	1.5887	3.0619		5	1.1881	3.7976
			5.0580				6.4696
			7.0426				9.1253
			9.0440				11.7842
11.0	1	.02381		14.0	1	.01475	
	2	.4819	8.2769		2	.3744	10.5009
	3	.7988	5.2578		3	.6188	6.5824
			9.2368				11.7220
	4	1.1122	3.9996		4	.8594	4.9400
			6.8545				8.6377
			9.6919				12.3106
	5	1.4244	3.3120		5	1.1003	4.0335
			5.5391				6.9197
			7.7534				9.7871
			9.9756				12.6560
12.0	1	.02006		15.0	1	.01288	
	2	.4397	9.0712		2	.3488	11.2378
	3	..7281	5.6968		3	.5756	7.0269
			10.0631				12.5516
	4	1.0125	4.3121		4	.7991	5.2557
			7.4490				9.2337
			10.5664				13.1844
	5	1.3023	3.5395		5	1.0203	4.2854
			5.9757				7.3983
			8.3978				10.4913
			10.8164				13.5830

TABLE III

EIGENVALUES AND NODES FOR THE EXTENSIONAL MODES OF FREE VIBRATION OF A UNIFORM ANNULAR DISK. POISSON'S RATIO: $\nu = 0.3$

Diam. Ratio $\frac{b}{a}$	Mode n	Eigen-values λ_n	Nodes	Diam. Ratio $\frac{b}{a}$	Mode n	Eigen-values λ_n	Nodes
2.0	1	1.5920		7.0	1	.3041	
	2	4.7292	1.6711		2	.8253	5.1124
	3	7.9059	1.3992		3	1.3391	3.4665
			1.7989				5.8362
3.0	1	.8314			4	1.8556	2.7534
	2	2.3898	2.3488				4.4614
	3	3.9493	1.8059				6.1608
			2.6056		5	2.3711	2.3600
	4	5.4404	1.5820				3.6949
			2.1614				5.0246
			2.7475				6.3535
4.0	1	.5733		8.0	1	.2639	
	2	1.6101	3.0332		2	.7117	5.8122
	3	2.6649	2.2149		3	1.1516	3.8909
			3.4110				6.6460
	4	3.6877	1.8643		4	1.5951	3.0323
			2.7208				5.0412
			3.5750				7.0187
5.0	1	.4408			5	2.0471	2.5832
	2	1.2191	3.7227				4.1307
	3	1.9926	2.6285				5.6706
			4.2181				7.2072
	4	2.7709	2.1582	9.0	1	.2330	
			3.2997		2	.6261	6.5129
			4.4381		3	1.0110	4.3172
6.0	1	.3596					7.4591
	2	.9831	4.4170		4	1.3978	3.3578
	3	1.6004	3.0464				5.6278
			5.0274				7.8842
	4	2.2213	2.4551		5	1.7882	2.8227
			3.8804				4.5950
			5.2993				6.3588
	5	2.8461	2.1270				8.1410
			3.2378				
			4.3438				
			5.4561				

TABLE III (CONTINUED)

Diam. Ratio $\frac{b}{a}$	Mode n	Eigen-values λ_n	Nodes	Diam. Ratio $\frac{b}{a}$	Mode n	Eigen-values λ_n	Nodes
10.0	1	.2088		13.0	1	.1596	
	2	.5593	7.2139		2	.4242	9.3276
	3	.9012	4.7463		3	.6809	6.0432
			8.2721				10.7127
	4	1.2451	3.6631		4	.9385	4.5892
			6.2124				7.9746
			8.7472				11.3369
	5	1.5854	3.0663		5	1.2018	3.7639
			5.0668				6.4052
			7.0562				9.0310
			9.0550				11.6558
11.0	1	.1893		14.0	1	.1479	
	2	.5054	7.9180		2	.3929	10.0286
	3	.8133	5.1768		3	.6301	6.4755
			9.0845				11.5221
	4	1.1228	3.9692		4	.8678	4.0189
			6.7974				8.5618
			9.6079				12.1989
	5	1.4339	3.2959		5	1.1054	4.0189
			5.5083				6.8918
			7.7085				9.7465
			9.9204				12.6037
12.0	1	.1733		15.0	1	.1381	
	2	.4613	8.6208		2	.3660	10.7310
	3	.7411	5.6097		3	.5860	6.9141
			9.8999				12.3413
	4	1.0224	4.2780		4	.8068	5.2126
			7.3846				9.1520
			10.4710				13.0640
	5	1.3061	3.5319		5	1.0311	4.2488
			5.9618				7.3292
			8.3777				10.3895
			10.7954				13.4470

TABLE IV

EIGENVALUES AND NODES FOR THE EXTENSIONAL MODES OF FREE VIBRATION OF A UNIFORM ANNULAR DISK. POISSON'S RATIO: $\nu = 0.5$

Diam. Ratio $\frac{b}{a}$	Mode n	Eigen-values λ_n	Nodes	Diam. Ratio $\frac{b}{a}$	Mode n	Eigen-values λ_n	Nodes
2.0	1	1.6553		7.0	1	.3213	
	2	4.7503	1.6680		2	.8308	5.0837
	3	7.9637	1.3965		3	1.3426	3.4598
			1.7931				5.8231
3.0	1	.8725			4	1.8588	2.7545
	2	2.4035	2.3411				4.4552
	3	3.9575	1.8043				6.1514
			2.6021		5	2.3590	2.3670
	4	5.4455	1.5816				3.7090
			2.1610				5.0448
			2.7416				6.3716
4.0	1	.6037		8.0	1	.2787	
	2	1.6203	3.0200		2	.7167	5.7763
	3	2.6512	2.2120		3	1.1547	3.8827
			3.4052				6.6323
	4	3.6896	1.8637		4	1.5970	3.0508
			2.7196				5.0361
			3.5733				7.0115
5.0	1	.4651			5	2.0518	2.5794
	2	1.2269	3.7043				4.1232
	3	1.9973	2.6242				5.6604
			4.2103				7.2010
	4	2.7779	2.1551	9.0	1	.2463	
			3.2939		2	.6308	6.4695
			4.4272		3	1.0137	4.3078
6.0	1	.3795					7.4411
	2	.9898	4.3926		4	1.3998	3.3543
	3	1.6047	3.0402				5.6212
			5.0166				7.8744
	4	2.2255	2.4521		5	1.7835	2.8273
			3.8745				4.6044
			5.2906				6.3729
	5	2.7995	2.1460				8.1652
			3.2759				
			4.4004				
			5.5391				

TABLE IV (CONTINUED)

Diam. Ratio $\frac{b}{a}$	Mode n	Eigen-values λ_n	Nodes	Diam. Ratio $\frac{b}{a}$	Mode n	Eigen-values λ_n	Nodes
10.0	1	.2209		13.0	1	.1686	
	2	.5632	7.1682		2	.4273	9.2632
	3	.9036	4.7362 / 8.2528		3	.6829	6.0280 / 10.6840
	4	1.2470	3.6587 / 6.2036 / 8.7336		4	.9400	4.5827 / 7.9626 / 11.3199
	5	1.5885	3.0624 / 5.0584 / 7.0444 / 9.0199		5	1.1905	3.7914 / 6.4582 / 9.1086 / 11.7529
11.0	1	.2002		14.0	1	.1565	
	2	.5089	7.8677		2	.1357	9.9626
	3	.8157	5.1641 / 9.0606		3	.6317	6.4609 / 11.4851
	4	1.1240	3.9663 / 6.7910 / 9.5982		4	.8689	4.8940 / 8.5510 / 12.1834
	5	1.4350	3.2939 / 5.5044 / 7.7031 / 9.9043		5	1.1054	4.0189 / 6.8918 / 9.7465 / 12.6037
12.0	1	.1830		15.0	1	.1459	
	2	.4644	8.5665		2	.3683	10.6657
	3	.7434	5.5944 / 9.8706		3	.5876	6.8974 / 12.3102
	4	1.0236	4.2740 / 7.3771 / 10.4610		4	.8080	5.2062 / 9.1397 / 13.0466
	5	1.3030	3.5384 / 5.9739 / 8.3951 / 10.8161		5	1.0268	4.2631 / 7.3562 / 10.4305 / 13.5048

APPENDIX B

TABLE V

SUPERPOSITION INTEGRAL FORMULAS

a) $\displaystyle\int_0^t \sin n(t-\tau)\,d\tau = \frac{1}{n}\left[\cos n(t-\tau)\right]_0^t = \frac{1}{n}(1-\cos nt)$

b) $\displaystyle\int_0^t \tau \sin(t-\tau)\,d\tau = \frac{1}{n^2}\left[\sin n(t-\tau)+n\tau\cos n(t-\tau)\right]_0^t = \frac{1}{n^2}(nt-\sin t)$

c) $\displaystyle\int_0^t \tau^2 \sin n(t-\tau)\,d\tau = \frac{1}{n^3}\left[(n^2\tau^2-2)\cos n(t-\tau)+2n\tau\sin n(t-\tau)\right]_0^t$

$$= \frac{1}{n^3}(n^2 t^2 - 2 + 2\cos nt)$$

d) $\displaystyle\int_0^t \sin m\tau \sin n(t-\tau)\,d\tau = \frac{1}{2}\left[-\frac{\sin[m\tau+n(t-\tau)]}{m-n}+\frac{\sin[m\tau-n(t-\tau)]}{m+n}\right]_0^t$

$$= \frac{m\sin nt - n\sin mt}{m^2-n^2}$$

e) $\displaystyle\int_0^t \tau \sin m\tau \sin n(t-\tau)\,d\tau = \left[\frac{\tau}{2}\left(-\frac{\sin[m\tau+n(t-\tau)]}{m-n}+\frac{\sin[m\tau-n(t-\tau)]}{m+n}\right)\right.$

$$\left.-\frac{1}{2}\left(\frac{\cos[m\tau+n(t-\tau)]}{(m-n)^2}+\frac{\cos[m\tau-n(t-\tau)]}{(m+n)^2}\right)\right]_0^t$$

$$= t\left(\frac{m\sin nt - n\sin mt}{m^2-n^2}\right)-\frac{m^2+n^2}{(m^2-n^2)^2}(\cos mt - \cos nt)$$

f) $\displaystyle\int_0^t \cos m\tau \sin n(t-\tau)\,d\tau = \frac{1}{2}\left[-\frac{\cos[m\tau+n(t-\tau)]}{m-n}+\frac{\cos[m\tau-n(t-\tau)]}{m+n}\right]_0^t$

$$= n\left(\frac{\cos nt - \cos mt}{m^2-n^2}\right)$$

g) $\displaystyle\int_0^t \sin^2 m\tau \sin n(t-\tau)\,d\tau = \left[\frac{\cos n(t-\tau)}{2n}+\frac{\cos[2m\tau+n(t-\tau)]}{4(2m-n)}-\frac{\cos[2m\tau-n(t-\tau)]}{4(2m+n)}\right]_0^t$

$$= \frac{1-\cos nt}{2n}+\frac{1}{2}\cdot\frac{n}{4m^2-n^2}(\cos 2mt - \cos nt)$$

BIBLIOGRAPHY

BIBLIOGRAPHY

STRESSES AND FREE VIBRATION OF NON-ROTATING DISKS

1. Aggarwal, R.R. "Axially Symmetric Vibrations of a Finite Isotropic Disk," Journal of the Acoustic Society of America. 24:463-7, September, 1952.

2. Deresiewicz., H., and R.D.Mindlin. "Axially Symmetric Flexual Vibrations of a Circular Disk," Journal of Applied Mechanics. 22:86-8, March, 1955.

3. Gazis, D.C., and R.D.Mindlin."Extensional Vibrations and Waves in a Circular Disk and a Semi-Infinite Plate," Journal of Applied Mechanics.27:541-7, September,1960.

4. Kane, T.R., and R.D.Mindlin. "High Frequency Extensional Vibrations of Plates," Journal of Applied Mechanics. 23:277-83, June, 1956.

5. Love, A.E.H. A Treatise on the Mathematical Theory of Elasticity. Fourth edition. New York:Dover,1944.

6. Mindlin, R.D., and H. Deresiewicz. "Thickness-Shear and Flexural Vibrations of a Circular Disk," Journal of Applied Physics. 25:1329-32, October, 1954.

7. Moseley, D.S. "Contribution to the Theory of Radial Extensional Vibrations in Thin Disks," Journal of the Acoustical Society of America. 32:991-5, August, 1960.

8. Nowak, M.J."The Simplest Extensional Vibration of a Circular Disk," Journal of Applied Mechanics. 29:437-9, June 1962.

9. Raju, P.N."Vibrations of Annular Plates," Journal of the Aeronautical Society of India. 14:37-52, May 1962.

10. Rayliegh, J.W. Strutt, Baron. Theory of Sound, V.I. Second edition.London: Macmillan, 1894.

11. Sharma, R.L. "Dependence of Frequency Spectrum of a Circular Disk on Poisson's Ratio," Journal of Applied Mechanics. 24:53ff., March, 1957.

12. Shaw, E.A.G. "On the Resonant Vibrations of Thick Barium Titanate Disks, "Journal of the Acoustical Society of America. 28:38-50, 1956.

STRESSES AND FREE VIBRATIONS IN ROTATING DISKS

13. Biezeno, C.B., and R. Grammel. Steam Turbines, V. III of Engineering Dynamics. 4 vols. Trans. E.F.Winter and H.A.Havemann. New York: D.Van Nostrand, 1954.

14. Frost, T.H., and K.F. Whitcomb. "Stresses in Rotating Disks," Transactions of the ASME. 53:1ff, 1931.

15. Guernsey, R. "Photoelastic Study of Centrifugal Stresses in a Single Wheel and Hub,"Experimental Mechanics. 1:1-7,1961.

16. Hetenyi, M. "Some Applications of Photoelasticity in Turbine-Generator Design," Journal of Applied Mechanics. 6, 1939.

17. Karas, K. "Strain and Deformation in a Rotating Disk Subject to Axial Torsional Moments," Ing.-Arch. 30:63-76, January, 1961.

18. Ku, Ta-Chang. "Stress Concentration in a Rotating Disk With a Central Hole and Two Additional Symmetrically Located Holes," Journal of Applied Mechanics. 27: 359-60.

19. Lamb, H., and R.V. Southwell. "Vibration of a Spinning Disc," London Royal Society Proceedings, (Ser.A) 99:272ff, 1921.

20. Newton,R.E. "A photoelastic Study of Stresses in Rotating Disks," Journal of Applied Mechanics. 7, 1940.

21. Owen, M.J. "An Elastoplastic Analysis of a Rotating Disk," Journal of the Franklin Institute. 267:55-68, January, 1958.

22. Simmonds, J.G. "The In-Plane Vibrations of a Flat Spinning Disk," NASA Technical Note, number D-521 (corrected copy). December, 1962.

23. Singh, B.R., and N.S. Nandeeswaraiya. "Vibration Analysis of a Turbine Disc in its Plane," Journal of Science and Engineering Research (India). 1:157-60, July, 1956.

24. Southwell, R.V. "Free Transverse Vibrations of a Uniform Circular Disc Clamped at its Centre," London Royal Society Proceedings. (Ser.A). 101:131ff, 1922.

25. Timoshenko,S., and J.N.Goodier. Theory of Elasticity. Second edition. New York: McGraw-Hill, 1951.

EXPERIMENTAL TECHNIQUES

26. Dally, J.W., W.F. Riley, and A.J.Durelli." A Photoelas-
     tic Approach to Transient Stress Problems Employing
     Low-Modulus Materials," Journal of Applied Mechanics.
     26:613-20, December, 1959.

27. Dolan, T.J., W.M. Murray, and D.C.Drucker. "Photoelas-
     ticity," Handbook of Experimental Stress Analysis,
     M.Hetenyi, editor. New York: J.Wiley and Sons, 1950.
     Pp. 828-976.

28. Drucker, D.C "Photoelastic Separation of Principal
     Stresses by Oblique Incidence," Journal of Applied
     Mechanics. 10:156-60, September, 1943.

29. Durelli, A.J., J.W.Dalley, and W.F.Riley. "Developments
     in the Application of the Grid Method to Dynamics
     Problems," Journal of Applied Mechanics. 26:629-34,
     December, 1959.

30. Findley, W.N. "The Fundamentals of Photoelastic Stress
     Analysis Applied to Dynamic Stresses," Proceedings of
     the 9th Semi-Annual Photo-elasticity Confrence, 1939,
     pp. 1-11.

31. Goldsmith, W. "Dynamic Photoelasticity," Experimental
     Techniques in Shock and Vibration. A publication
     from the Winter Annual Meeting of the ASME, November,
     1962, pp. 25-54.

32. Perkins,H.C. "Movies of Stress Waves in Photoelastic
     Rubber," Journal of Applied Mechanics. 20:140-1,
     March, 1953.

33. Riley,W.F., and A.J. Durelli. "Stress Distribution on
     the Boundary of a Circular Hole in a Large Plate
     During Passage of a Stress Pulse of Long Duration,"
     Journal of Applied Mechanics. 28:245-51, September,
     1961.

OTHER REFERENCES

34. Christie, D.G. "Reflection of Elastic Waves from a Free Boundary," Philosophical Magazine, 46:527-41, 1955.

35. Churchill, R.V. Operational Mathematics. Second edition. New York: McGraw-Hill, 1958.

36. Folk, Robert, et al. "Elastic Strain Produced by Sudden Application of Pressure to One End of a Cylindrical Bar- I. Theory," Journal of the Acoustical Society of America, 30:552-58, June, 1958.

37. Jahnke, E., and F.Emde. Tables of Functions. Fourth edition.New York: Dover, 1945.

38. Jones,E.O. and A.T.Ellis. "Longitudinal Strain Pulse Propagation in Wide Rectangular Bars," Journal of Applied Mechanics. 30:51-60, March, 1963.

39. Kolsky, H. Stress Waves in Solids. London: Oxford Press, 1953.

40. Sneddon, I.N. Fourier Transforms. New York: McGraw-Hill, 1951.

41. Wylie, C.R. Advanced Engineering Mathematics. Second edition. New York: McGraw-Hill, 1960.

ABSTRACT

The object of this thesis was to lay a foundation
for a comprehensive study, both theoretical and experimental,
of the transient response of rotating members.

An analysis was made of the stresses and in-plane
displacements of a uniform annular rotating disk, clamped to
a rigid shaft and subjected to transient shaft inputs. The
solution was obtained from two-dimensional theory of
elasticity by the method of generalized integral transforms
in terms of superposition integrals, so that any integrable
function could be chosen for the shaft inputs. Three in-
puts were selected and the integrals evaluated.

The first five natural frequencies and nodes were de-
termined numerically for the free torsional and extensional
modes of in-plane vibration. It was concluded that the
effect of rotation on the natural frequencies was negligible.
The numerical data is sufficient for numerical determination
of stresses and displacements for comparison with experimen-
tal results.

A survey is made of some techniques of dynamic photo-
elasticity used in experimental investigation of transient
phenomena. Two new techniques are proposed, one combining
normal and oblique incidence polariscopes into one instrument,
the other combining an interferometer and polariscope, so

that simultaneous photographs of two independent optical interference patterns may be obtained as a means of eliminating the need for the exact reproduction of transient response phenomena.

A discussion is presented of the problem of dynamic similarity in dynamic problems. The equations of motion are non-dimensionalized and two dimensionless parameters are introduced, which make it possible to generalize the experimental results more fully and apply them to rotating members constructed of any material.

Sept. 3, 1963   **APPROVED:**
_____
        Date